

High levels of auxin signalling define the stem-cell organizer of the vascular cambium

Ondřej Smetana^{1,2}, Riikka Mäkilä^{1,2}, Munan Lyu^{1,2}, Ali Amiryousefi², Filomeno Sánchez Rodríguez^{1,2}, Miin-Feng Wu³, Anna Solé-Gil^{1,2}, Marina Leal Gavarrón^{1,2}, Riccardo Siligato^{1,2}, Shunsuke Miyashima^{1,2}, Paweł Roszak^{1,2,4}, Tiina Blomster^{1,2}, Jason W. Reed³, Suvi Broholm^{1,2} & Ari Pekka Mähönen^{1,2*}

Wood, a type of xylem tissue, originates from cell proliferation of the vascular cambium. Xylem is produced inside, and phloem outside, of the cambium¹. Morphogenesis in plants is typically coordinated by organizer cells that direct the adjacent stem cells to undergo programmed cell division and differentiation. The location of the vascular cambium stem cells and whether the organizer concept applies to the cambium are currently unknown². Here, using lineage-tracing and molecular genetic studies in the roots of *Arabidopsis thaliana*, we show that cells with a xylem identity direct adjacent vascular cambial cells to divide and function as stem cells. Thus, these xylem-identity cells constitute an organizer. A local maximum of the phytohormone auxin, and consequent expression of CLASS III HOMEODOMAIN-LEUCINE ZIPPER (HD-ZIP III) transcription factors, promotes xylem identity and cellular quiescence of the organizer cells. Additionally, the organizer maintains phloem identity in a non-cell-autonomous fashion. Consistent with this dual function of the organizer cells, xylem and phloem originate from a single, bifacial stem cell in each radial cell file, which confirms the classical theory of a uniseriate vascular cambium³. Clones that display high levels of ectopically activated auxin signalling differentiate as xylem vessels; these clones induce cell divisions and the expression of cambial and phloem markers in the adjacent cells, which suggests that a local auxin-signalling maximum is sufficient to specify a stem-cell organizer. Although vascular cambium has a unique function among plant meristems, the stem-cell organizer of this tissue shares features with the organizers of root and shoot meristems.

Plant organs grow axially during primary development and then radially during secondary development. In many plant organs—including woody stems—secondary development is organized by two concentric, cylindrical meristems that undergo periclinal cell divisions (that is, the division plane is parallel to the surface of an organ or a tissue): the inner vascular cambium proliferates to produce conductive xylem and phloem, and the outer phellogen (also called cork cambium) produces protective tissue called phellem⁴. In the root of *A. thaliana*, secondary meristems originate from parenchymal cells located between primary xylem and phloem (a tissue known as procambium) and from cells surrounding the procambium, xylem and phloem, which form a tissue known as the pericycle^{5,6} (Fig. 1a, Extended Data Fig. 1a, b).

To understand, at cellular resolution, how the vascular cambium and phellogen develop from the procambium and pericycle, we designed a Cre-lox recombination system to carry out cell-lineage tracing in the *Arabidopsis* root (Extended Data Fig. 2a, b). Clones marked by expression of β -glucuronidase (GUS) were induced during the activation of root secondary growth (Fig. 1a, b), and the subsequent sectors were analysed after 11 days. GUS sectors showed highly repetitive patterns that indicated that the secondary development is a tightly controlled process (Fig. 1b, Extended Data Fig. 2c). This enabled us to develop a fate map of procambial and pericycle cells during the morphogenesis

of root secondary tissue (Fig. 1b). The fate map showed that phellogen originates from the pericycle (dark and light purple, in Fig. 1b), confirming previous anatomical observations^{4–6}. Pericycle cells adjacent to the primary xylem (xylem-pole pericycle (XPP) cells, dark purple in Fig. 1b) are also the founder cells of the vascular cambium. The proliferation of XPP cells thus leads to the separation of the two concentric meristems and production of all the secondary tissues from their circumferential position (Extended Data Fig. 2d). Our finding underscores the pluripotency of XPP cells, which are also the source of lateral roots and regenerated tissue (callus)⁷. The fate map also revealed that only those procambial cells that are in physical contact with primary xylem vessels (red, in Fig. 1b) give rise to vascular cambium, secondary xylem, and phloem. Thus, these xylem-adjacent procambial cells, together with xylem-adjacent daughters of XPP cells, act as the stem cells of vascular cambium during the activation of secondary growth. The fact that procambial and pericycle cells that are not in contact with xylem (pink and light purple, respectively, in Fig. 1b) do not form vascular cambium suggests that cellular position (that is, being adjacent to xylem), rather than identity during primary development, determines the origin of the vascular cambium. This conclusion is further supported by lineage tracing in roots that have transiently been treated with the phytohormone cytokinin, which imparts procambium identity to cells in the protoxylem position. These cells are located adjacent to the remaining xylem and formed only vascular cambium, whereas cells in the XPP position—no longer adjacent to xylem cells—formed only phellogen and not vascular cambium (Extended Data Fig. 2d–g). Together, these findings suggest that xylem or xylem precursor cells cause neighbouring cells to become vascular cambium stem cells.

At the onset of secondary growth (Fig. 1a), primary xylem cells have already undergone programmed cell death as the final step of their differentiation. We therefore hypothesized that xylem induces stem-cell identity in the neighbouring cells earlier, during primary development, when cells with xylem identity are alive and capable of signal transduction. A family of five redundantly acting HD-ZIP III transcription factors determine xylem identity during the primary development of the *Arabidopsis* root^{8–10}. Additionally, an HD-ZIP III orthologue in *Populus* regulates vascular cambium morphogenesis¹¹. HD-ZIP III transcription factors are thus likely candidates for regulating signals for stem-cell identity. HD-ZIP III transcription factors are expressed in the cambial zone; *AtHBS8* at least is expressed predominantly on the xylem side of the vascular cambium, adjacent to the cells undergoing cell division (highlighted with expression of AINTEGUMENTA (ANT)), which is consistent with the idea that genes for HD-ZIP III transcription factors mark cells with secondary xylem identity (Fig. 2a, Extended Data Fig. 3a, b). Only mutants that lack at least four of the HD-ZIP III family genes show patterning defects and reduced xylem formation in the primary root vasculature⁸. The same mutant combinations also show scattered cambial divisions and xylem patterning during secondary development (Extended Data Fig. 3c, d). To examine whether these

¹Institute of Biotechnology, HiLIFE, University of Helsinki, Helsinki, Finland. ²Organismal and Evolutionary Biology Research Programme, Faculty of Biological and Environmental Sciences, Viikki Plant Science Centre, University of Helsinki, Helsinki, Finland. ³Department of Biology, University of North Carolina at Chapel Hill, Chapel Hill, NC, USA. ⁴The Sainsbury Laboratory, University of Cambridge, Cambridge, UK. *e-mail: AriPekka.Mahonen@helsinki.fi

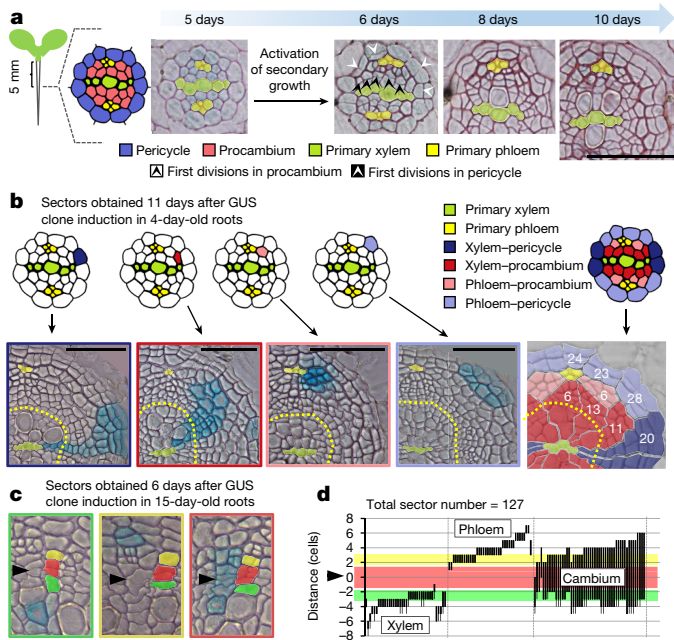


Fig. 1 | Lineage tracing revealed the origin of the vascular cambium stem cells. **a**, The activation of secondary root growth is characterized by the initiation of periclinal cell divisions in procambial cells (black arrowheads), followed by divisions in pericycle (white arrowheads), leading to the formation of vascular cambium and phellogen. Cell divisions are marked only in top half of the cross-section. **b**, Lineage tracing initiated from the primary vasculature (top) showed the importance of an initial xylem connection for the ontogeny of the cambium (yellow dashed line). The bottom panel shows the four major types of clonal sectors obtained. Frames are coloured to match the corresponding cell lineages in the top panels. The numbers in the fate map (bottom right) refer to the observed number of the sectors. **c**, **d**, Lineage tracing in active cambium revealed a common stem cell for xylem and phloem. GUS sectors (black bars) plotted on the basis of the position of thinnest cell wall (arrow) in each radial file, which represents the most recent periclinal cell division in cambium ($y = 0$). Scale bars, 50 μm . All experiments were repeated four times.

severe developmental defects are a direct consequence of the loss of HD-ZIP III transcription factors or a secondary consequence of defects in primary development, we constructed a line with an inducible¹² miR165a, a microRNA (miRNA) that targets the mRNAs of all five HD-ZIP III transcription factors¹³ (Extended Data Fig. 4a). Ubiquitous induction of miR165a from germination onwards led to severe inhibition of primary xylem differentiation (Extended Data Fig. 4b), similar to the phenotype of the quintuple HD-ZIP III mutant⁸. Induction of miR165a during the activation of secondary growth initially blocked vessel differentiation, which indicates that the HD-ZIP III transcription factors are also required for secondary xylem-vessel formation (Fig. 2b). Dispersed cell divisions and erratic xylem-vessel formation occurred in the remaining undifferentiated tissue, resembling the phenotypes of quadruple HD-ZIP III mutants (Extended Data Fig. 3d). Induction of miR165a during secondary growth forced xylem parenchyma cells and cells with xylem identity—which were previously quiescent—to re-enter mitosis, generating a population of dividing cells in the place of xylem (Fig. 2c, Extended Data Fig. 4c). These results indicate that the HD-ZIP III transcription factors are required for cellular quiescence in xylem cells. *WUSCHEL-RELATED HOMEBOX 4* (*WOX4*)¹⁴ and *PHLOEM INTERCALATED WITH XYLEM* (*PXY*, also known as *TDIF RECEPTOR* (*TDR*))^{14,15} are key cambial regulators. They show expression maxima on the xylem-side of the cambium and weak expression in the adjacent dividing cells (marked with *ANT* expression), which strongly resembles the expression pattern of *AtHB8* (Fig. 2a). Induction of miR165a led to downregulation of *WOX4*, *PXY* and *ANT* (Fig. 2d,

Extended Data Fig. 4d). These data imply that xylem-identity regulators—the HD-ZIP III transcription factors—define a stem-cell organizer that confers cambium stem-cell identity to the adjacent cells, in a non-cell-autonomous manner.

The loss of the HD-ZIP III transcription factors also caused decreased production of differentiated phloem cells (Extended Data Fig. 4e) and lower expression of the early phloem marker *PHLOEM-EARLY-DOF 1* (*PEAR1*)^{16,17} (Fig. 2a, d, Extended Data Figs 1a, 4d), which suggests that the organizer cells maintain a common stem cell for secondary xylem and phloem. To test this hypothesis, we traced cell lineages during secondary growth. GUS clones were generated in 15-day-old or 30-day-old *Arabidopsis* roots, which contain 2–4 (at 15 days old) or 7–9 (at 30 days old) layers of vascular cambial cells that could histologically be identified (Extended Data Fig. 1b). In each radial cell file, three different types of GUS sectors were observed (Fig. 1c, Extended Data Fig. 5a–c). GUS clones that originated from the xylem (green) or phloem (yellow) side of the cambium differentiated into the corresponding cell types or divided before differentiation. By contrast, cells located in the centre of the cambium (red) produced broad GUS sectors that spanned into the differentiated xylem and phloem (Fig. 1c, d, Extended Data Fig. 5c, d). Similarly, induction of clones in the *ANT* expression domain—marking a narrow layer of dividing cells—led to production of GUS sectors that spanned in both directions (Fig. 2a, Extended Data Fig. 5e–h). These data demonstrate that the vascular cambium comprises a single, bifacial stem cell in each radial cell file, and that stem cells are marked with *ANT* expression. These stem cells produce both xylem and phloem—thus confirming the 145-year-old theory of the uniseriate vascular cambium^{3,4}, at least in the *Arabidopsis* root. This theory states that a single layer of ‘initials’ (stem cells) produces both xylem and phloem; and was later elaborated upon by the observation that the position of the initials varied between neighbouring radial files^{1,4}. Our experimental data support these later modifications; the variable location of the stem cells can be observed as a considerable radial distribution of the GUS sectors that originate from stem cells (Fig. 1d, Extended Data Fig. 5d).

To test whether the HD-ZIP III transcription factors are sufficient to induce the formation of an ectopic organizer within the cambium, we inducibly overexpressed a version of *AtHB8* (termed *AtHB8d*) that was resistant to all miR165 and miR166 miRNAs, in the stem-cell domain under the *ANT* promoter¹². Induction of *pANT:XVE >> AtHB8d-YFP* rapidly inhibited cell division in the stem cells, thus confirming the ability of the HD-ZIP III transcription factors to promote cellular quiescence (Extended Data Fig. 6a–c). This local quiescence was associated with a centrifugal shift—that is, towards phloem—in the domain of high cell division and organizer marker expression (Extended Data Fig. 6b, d), followed by the formation of ectopic xylem vessels in the cambium (Extended Data Fig. 6e). These data demonstrate that, of the HD-ZIP III family genes, at least *AtHB8* is sufficient to induce organizer function within the vascular cambium.

Auxin promotes expression of HD-ZIP III transcription factors in vascular tissues during primary development, and their expression often correlates with auxin signalling maxima^{18,19}. Because the auxin maximum reaches a peak on the xylem-side of tree vascular cambium^{20,21}, we next studied the pattern of the response to auxin signalling in the *Arabidopsis* root cambium. Auxin response markers showed a local maximum in the xylem domain, and tapered off towards the cambium stem cells, which resembles the expression pattern of *AtHB8*, *WOX4* and *PXY* (Figs 2a, 3a, Extended Data Fig. 7a, b). Auxin signalling is mediated by AUXIN RESPONSE FACTOR (ARF) transcription factors²². We focused our expression analysis on class A ARFs, because their activity is preferentially auxin-regulated²²; *MONOPTEROS* (*MP*) (also known as *ARF5*), a class A ARF, has previously been shown to regulate normal vascular formation²³ and cambium-cell division by controlling the expression of *WOX4*²⁴. Of the five class A ARFs, three (*MP*, *ARF7* and *ARF19*) showed strong and consistent expression in the vascular cambium (Extended Data Fig. 7c, d). Because the *arf7 arf19* double mutant did not show clear patterning defects (Extended Data

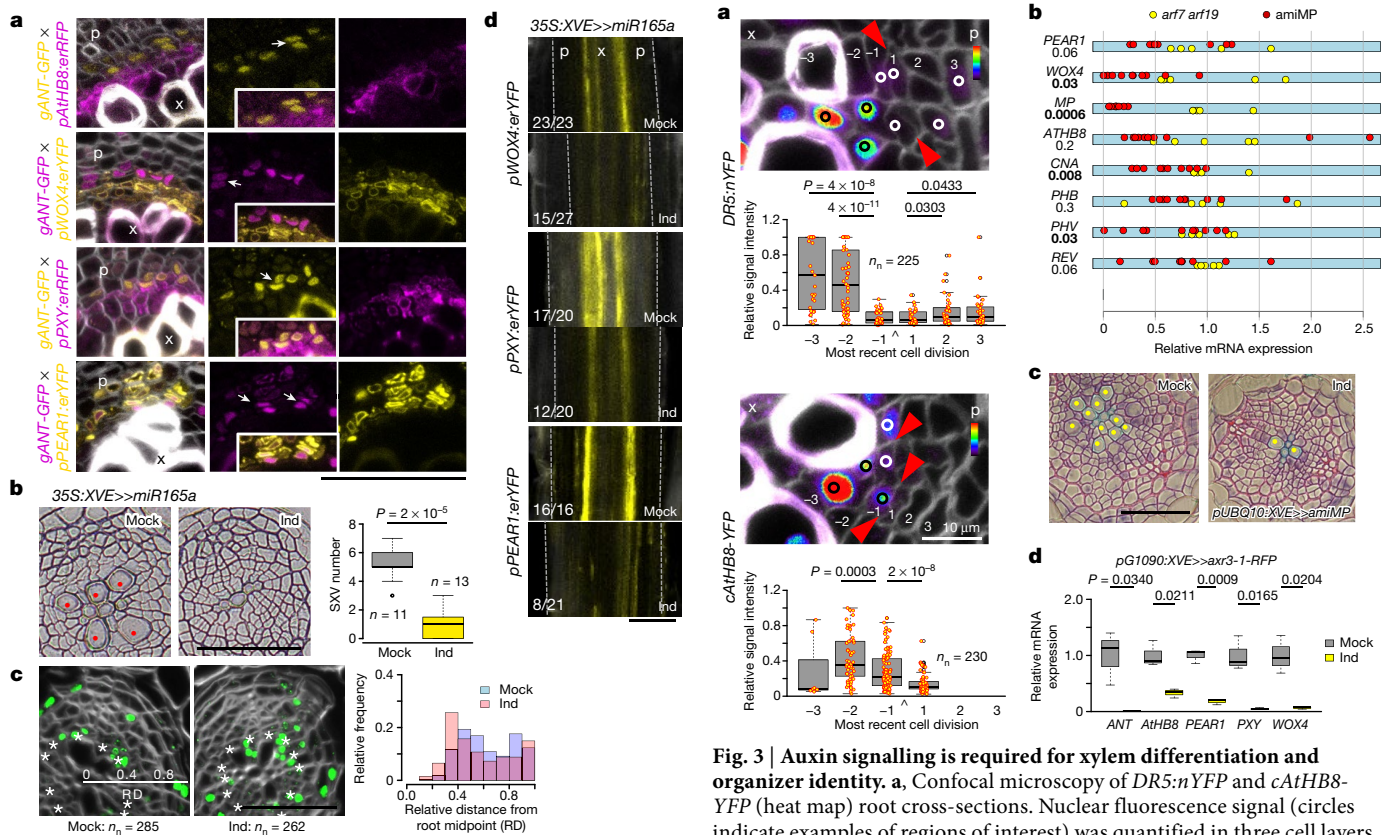


Fig. 2 | HD-ZIP IIIs determine the organizer of the vascular cambium. **a**, Confocal microscopy of cross-sections of *ANT* double markers in 14-day-old plants. White arrows indicate pairs of nuclei in recently dividing cells. Insets, merged reporter channels. **b**, Bright-field microscopy of root after miR165a induction (Ind) for 6 days (in 5-day-old plants). Red dots, secondary xylem vessels (SXV); quantification presented on the right. Box-and-whisker plot shows median and interquartile range; whiskers show range, dots show outliers. Two-tailed Wilcoxon test; *n*, independent roots. **c**, Confocal microscopy of roots after 5-ethynyl-2'-deoxyuridine (EdU) staining to detect S-phase nuclei reveal a centripetal shift of the cell division domain after a 2-day miR165a induction (in 8-day-old plants). Asterisks mark cambium. Histograms showing the relative distances of EdU-positive nuclei in the radial direction from the root midpoint (xylem axis: *x* = 0; root surface, *x* = 1), as depicted in mock. *n_n*, total number of nuclei. RD, relative distance from root midpoint. **d**, Confocal microscopy of fluorescent markers after 2-day miR165a induction (in 8-day-old plants). Dashed lines, borders of the secondary tissues. The numbers in the bottom left corner of subpanels represent the frequency of the observed phenotype. **a**, **c**, **d**, Cell wall staining in grey. p, phloem; x, xylem. All experiments were repeated at least three times. Scale bars, 50 μm.

Fig. 8a), and strong *mp* mutants failed to initiate roots²⁵, we developed an inducible artificial miRNA (amiRNA) line that targets *MP*—which we name amiMP—in the *arf7 arf19* background. Ubiquitous induction of amiMP led to a reduction in transcript levels of *MP*, downregulation of *WOX4* and a subset of genes for HD-ZIP III transcription factors, and a reduction in secondary vessel formation (Fig. 3b, c, Extended Data Fig. 8b, c), similar to the miR165a-overexpression phenotype (Fig. 2b). Similarly, ubiquitous induction of an inducible, stable ARF-signalling repressor *axr3-1* (ref. 26) led to a strong downregulation of the organizer, stem-cell and phloem-identity genes, as well as the genes of HD-ZIP III family, followed by termination of vascular cambium activity (Fig. 3d, Extended Data Fig. 8d–f). These data show that auxin signalling through transcription factors encoded by *MP*, *ARF7* and *ARF19*—and perhaps other ARF genes—promotes the expression of HD-ZIP III genes, *PXY* and *WOX4* in the stem-cell organizer, and that this signalling module is required to maintain vascular cambium identity. Because manipulations of levels of HD-ZIP III transcription

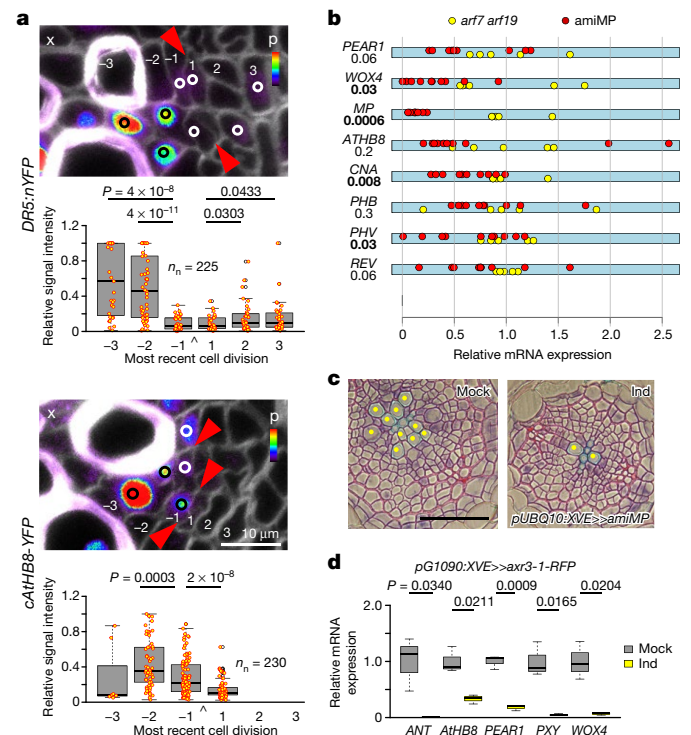


Fig. 3 | Auxin signalling is required for xylem differentiation and organizer identity. **a**, Confocal microscopy of *DR5:nYFP* and *cAtHB8-YFP* (heat map) root cross-sections. Nuclear fluorescence signal (circles indicate examples of regions of interest) was quantified in three cell layers from the most recent cell division (arrowheads in micrographs and on *x* axis) towards xylem (positions -1 , -2 and -3) and phloem (positions 1, 2 and 3). *n_n* = total number of nuclei. Cell wall staining in grey. p, phloem; x, xylem. **b**, Quantitative PCR with reverse transcription (qRT-PCR) analysis of marker-gene expression in amiMP T1 transformants in *arf7 arf19* background with the lowest level of *MP* transcripts. Each point represents an individual amiMP T1 transformant (*n* = 10) or individual *arf7 arf19* plant (*n* = 5) of the same age. The *P* values of a one-sided *t*-test comparing amiMP to *arf7 arf19* controls are provided under each gene name, and significant values are in bold. **c**, Bright-field microscopy of *pUBQ10:XVE >> amiMP* transformants in the *arf7 arf19* background induced for 7 days (in 5-day-old plants). Yellow dots, secondary xylem vessels. Experiment was repeated three times with similar results. **d**, qRT-PCR analysis of marker-gene expression in inducible *axr3-1* after 24h induction (in 8-day old plants). Data are from three experiments (*n* = 16 roots per treatment). In **a** and **d**, box-and-whisker plots show median and interquartile range; whiskers show range. One-tailed *t*-test. In **a**, dots represents independent data points. Scale bars, 10 μm (a), 50 μm (c).

factors lead to changes in auxin response (Extended data Fig. 7e–g), our data further suggest that ARF and HD-ZIP III transcription factors, and auxin, are under positive feedback regulation in the vascular cambium.

Finally, we tested whether the components that determine the stem-cell organizer are sufficient to induce vascular cambium formation when ectopically expressed. We generated activation clones in the phloem pole pericycle and surrounding cell files using an inducible S17 promoter^{12,16} (Extended Data Fig. 9a, b). Even though *AtHB8d* was sufficient to re-specify the organizer when overexpressed in stem cells of the vascular cambium, it was unable to induce xylem vessel formation or expression of cambial markers in the S17 domain (Extended Data Figs. 6, 9c, d). However, a proportion of clones expressing *MPΔ* (a dominant active version of *MP*²⁷) formed ectopic vessel elements and had periclinal cell divisions in the adjacent cells (Fig. 4a, Extended Data Fig. 9e, f). Time-course experiments revealed that *MPΔ* cell-autonomously induced *WOX4*, *PXY* and *AtHB8* expression, followed by differentiation of the clones into vessel elements (Fig. 4a, b). During differentiation into vessels, *MPΔ* clones induced ectopic expression

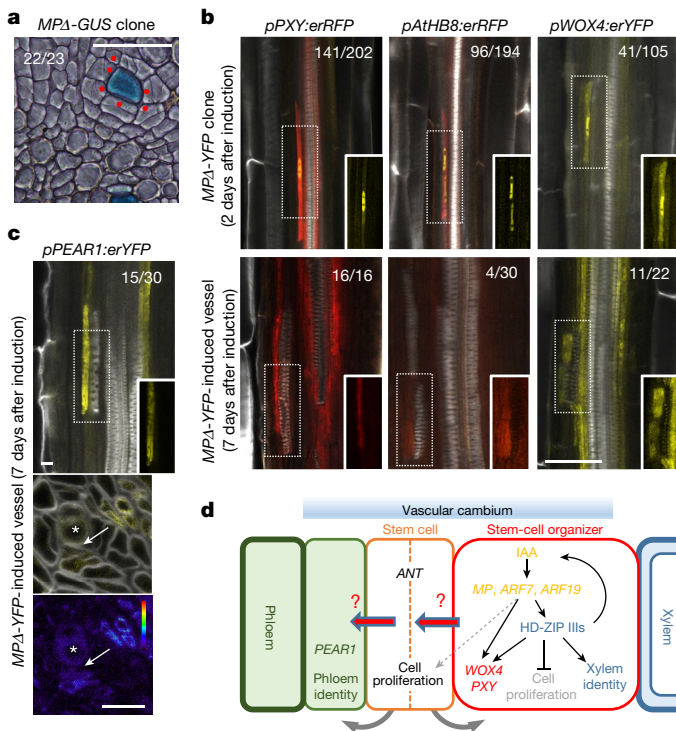


Fig. 4 | MP is sufficient for the formation of an ectopic organizer. **a**, Bright-field micrograph of an $MP\Delta$ -GUS clone with periclinal cell divisions induced cell-non-autonomously. Red dots, GUS-negative cells dividing periclinally around the $MP\Delta$ -GUS clone. **b**, Confocal analysis of marker expression within $MP\Delta$ -YFP clones (top) and around $MP\Delta$ -YFP-induced ectopic vessels (bottom). Cell wall staining in grey. Insets show YFP channel, except for insets of PXY and AtHB8 in bottom panels, which show RFP channel. **c**, PEAR1 is induced a few cell layers away from $MP\Delta$ -induced ectopic vessels (asterisk). An arrow indicates a gap between ectopic vessel and PEAR1 expression. **d**, A model illustrating how a local auxin maximum and downstream components define an organizer that positions the stem cell in the adjacent cell. Curved arrows represent bidirectional cell proliferation from the bifacial stem cell. The numbers in the left corner of subpanels represent the frequency of the observed phenotype. HD-ZIP IIIs, HD-ZIP III genes; IAA, indole-3-acetic acid. Scale bars, 10 μ m (c), 50 μ m (a, b).

of WOX4, PXY and AtHB8 in the adjacent cells, which indicates that MP can also promote organizer-cell identity in a cell-non-autonomous manner (Fig. 4b). Additionally, the early phloem marker PEAR1 appeared ectopically at a distance of a few cells from the clone, which suggests that the presence of an $MP\Delta$ clone is sufficient to promote the formation of a vascular cambium (Fig. 4c). $MP\Delta$ induces expression of the genes that define the stem-cell organizer before xylem vessel formation; this suggests that a cellular identity induced by high levels of auxin signalling, rather than the presence of xylem vessels, defines the organizer. Supporting this, clonal activation of VASCULAR-RELATED NAC-DOMAIN 6 (VND6)—which directly induces terminal differentiation of xylem vessels²⁸—failed to promote organizer-gene expression within the clone (Extended Data Figs. 1a, 9g). In the longer term, a proportion of VND6-induced vessels were surrounded by cells that express a subset of cambial markers; however, these cells rarely divided (Extended Data Fig. 9e, f). This indicates that the chemical or physical properties of terminally differentiated xylem vessels are not sufficient to induce organizer formation. Together, these data demonstrate that a locally high level of auxin signalling within root vascular tissue is sufficient to establish an organizer cell that promotes stem-cell-like divisions and identity in the adjacent cells (Fig. 4d). Our data reveal the dynamic nature of the organizer; differentiation of the organizer into a xylem vessel leads to formation of a new organizer in the adjacent cambial stem cell, thus ensuring the maintenance of the vascular cambium (Extended Data Fig. 10).

We uncovered a mechanistic framework that defines the stem-cell organizer of the vascular cambium (Fig. 4d). Similarly to the cells in the stem-cell organizer (quiescent centre) of the root apical meristem²⁹, the cells in the cambium organizer are quiescent and are defined by an auxin response maximum. However, unlike the root quiescent centre, the stem-cell organizer of the vascular cambium is dynamic: as the root grows thicker, organizer cells differentiate and stem cells acquire organizer identity (Extended Data Fig. 10a). Cells of the organizing centre of the shoot apical meristem also are replaced as they differentiate, although in this meristem the location of the organizer is stable. All three organizers express a member of the WOX gene family: WUSCHEL in the shoot apical meristem, WOX5 in the root meristem² and WOX4 in the vascular cambium, which underscores the related identity of cells in the three locations. Future challenges are to identify the cell-non-autonomous stem-cell factors that originate from the organizer cells (Fig. 4d), and to link other known cambial regulators³⁰ to the signalling module that defines the organizer (Extended Data Fig. 10).

Online content

Any methods, additional references, Nature Research reporting summaries, source data, statements of data availability and associated accession codes are available at <https://doi.org/10.1038/s41586-018-0837-0>.

Received: 15 June 2018; Accepted: 4 December 2018;
Published online 9 January 2019.

- Larson, P. R. *The Vascular Cambium: Development and Structure* (Springer, Berlin, 1994).
- Greb, T. & Lohmann, J. U. Plant stem cells. *Curr. Biol.* **26**, R816–R821 (2016).
- Sanio, C. Anatomie der gemeinen Kiefer (*Pinus silvestris* L.) II. Entwicklungsgeschichte der Holzellen. *Jahrb. Wiss. Bot.* **9**, 50–128 (1873).
- Evert, R. F. & Eichhorn, S. E. *Esau's plant anatomy: Meristems, Cells, and Tissues of the Plant Body—their Structure, Function and Development*, 3rd edn (John Wiley & Sons, Hoboken, 2006).
- Chaffey, N., Cholewa, E., Regan, S. & Sundberg, B. Secondary xylem development in *Arabidopsis*: a model for wood formation. *Physiol. Plant.* **114**, 594–600 (2002).
- Wunderling, A. et al. A molecular framework to study periderm formation in *Arabidopsis*. *New Phytol.* **219**, 216–229 (2018).
- Atta, R. et al. Pluripotency of *Arabidopsis* xylem pericycle underlies shoot regeneration from root and hypocotyl explants grown *in vitro*. *Plant J.* **57**, 626–644 (2009).
- Carlsbecker, A. et al. Cell signalling by microRNA165/6 directs gene dose-dependent root cell fate. *Nature* **465**, 316–321 (2010).
- Ohashi-Ito, K. & Fukuda, H. HD-Zip III homeobox genes that include a novel member, *ZeHb-13* (*Zinnia*)/*ATHB-15* (*Arabidopsis*), are involved in procambium and xylem cell differentiation. *Plant Cell Physiol.* **44**, 1350–1358 (2003).
- Baima, S. et al. The *Arabidopsis* ATHB-8 HD-zip protein acts as a differentiation-promoting transcription factor of the vascular meristems. *Plant Physiol.* **126**, 643–655 (2001).
- Robischon, M., Du, J., Miura, E. & Groover, A. The *Populus* class III HD ZIP, *popREVOLUTA*, influences cambium initiation and patterning of woody stems. *Plant Physiol.* **155**, 1214–1225 (2011).
- Siligato, R. et al. MultiSite gateway-compatible cell type-specific gene-inducible system for plants. *Plant Physiol.* **170**, 627–641 (2016).
- Mallory, A. C. et al. MicroRNA control of *PHABULOSA* in leaf development: importance of pairing to the microRNA 5' region. *EMBO J.* **23**, 3356–3364 (2004).
- Hirakawa, Y., Kondo, Y. & Fukuda, H. TDIF peptide signaling regulates vascular stem cell proliferation via the WOX4 homeobox gene in *Arabidopsis*. *Plant Cell* **22**, 2618–2629 (2010).
- Fisher, K. & Turner, S. PXY, a receptor-like kinase essential for maintaining polarity during plant vascular-tissue development. *Curr. Biol.* **17**, 1061–1066 (2007).
- Lee, J. Y. et al. Transcriptional and posttranscriptional regulation of transcription factor expression in *Arabidopsis* roots. *Proc. Natl Acad. Sci. USA* **103**, 6055–6060 (2006).
- Miyashima, S. et al. Mobile PEAR transcription factors integrate positional cues to prime cambial growth. *Nature* <https://doi.org/10.1038/s41586-018-0839-y> (2019).
- Ursache, R. et al. Tryptophan-dependent auxin biosynthesis is required for HD-ZIP III-mediated xylem patterning. *Development* **141**, 1250–1259 (2014).
- Donner, T. J., Sherr, I. & Scarpella, E. Regulation of preprocambial cell state acquisition by auxin signaling in *Arabidopsis* leaves. *Development* **136**, 3235–3246 (2009).
- Uggla, C., Moritz, T., Sandberg, G. & Sundberg, B. Auxin as a positional signal in pattern formation in plants. *Proc. Natl Acad. Sci. USA* **93**, 9282–9286 (1996).

21. Immanen, J. et al. Cytokinin and auxin display distinct but interconnected distribution and signaling profiles to stimulate cambial activity. *Curr. Biol.* **26**, 1990–1997 (2016).
22. Weijers, D. & Wagner, D. Transcriptional responses to the auxin hormone. *Annu. Rev. Plant Biol.* **67**, 539–574 (2016).
23. Przemeck, G. K., Mattsson, J., Hardtke, C. S., Sung, Z. R. & Berleth, T. Studies on the role of the *Arabidopsis* gene *MONOPTEROS* in vascular development and plant cell axialization. *Planta* **200**, 229–237 (1996).
24. Brackmann, K. et al. Spatial specificity of auxin responses coordinates wood formation. *Nat. Commun.* **9**, 875 (2018).
25. Berleth, T. & Jurgens, G. The role of the *monopteros* gene in organising the basal body region of the *Arabidopsis* embryo. *Development* **118**, 575–587 (1993).
26. Mähönen, A. P. et al. PLETHORA gradient formation mechanism separates auxin responses. *Nature* **515**, 125–129 (2014).
27. Krogan, N. T., Ckurshumova, W., Marcos, D., Caragea, A. E. & Berleth, T. Deletion of MP/ARF5 domains III and IV reveals a requirement for Aux/IAA regulation in *Arabidopsis* leaf vascular patterning. *New Phytol.* **194**, 391–401 (2012).
28. Kubo, M. et al. Transcription switches for protoxylem and metaxylem vessel formation. *Genes Dev.* **19**, 1855–1860 (2005).
29. Sabatini, S. et al. An auxin-dependent distal organizer of pattern and polarity in the *Arabidopsis* root. *Cell* **99**, 463–472 (1999).
30. Nieminen, K., Blomster, T., Helariutta, Y. & Mähönen, A. P. Vascular cambium development. *Arabidopsis Book* **13**, e0177 (2015).

Acknowledgements We thank T. Berleth, A. Carlsbecker, T. Greb, P. Ramachandran, E. Scarpella and D. Weijers for sharing published material; A.-M. Bågman, M. Herpola and J. Smetana for technical assistance; W. Yang for helping with the in situ protocol; and S. el-Showk, P. Etchells, Y. Helariutta, S. Otero and B. Scheres for constructive comments. This work was supported

by the Academy of Finland (grants #132376, #266431, #271832), University of Helsinki HiLIFE fellowship (O.S., R.M., M.L., A.S.G., F.S.R., M.L.G., R.S., T.B., S.B. and A.P.M.), Erasmus+ (F.S.R. and M.L.G.), and US National Science Foundation grant IOS-0744874 (M.-F.W. and J.W.R.).

Reviewer information *Nature* thanks T. Beeckman, H. Fukuda and J. Lohmann for their contribution to the peer review of this work.

Author contributions O.S. and A.P.M. designed the experiments. O.S. carried out all the experiments, except R.M. and M.L. conducted qRT-PCR, amiMP and inducible *axr3* work; F.S.R. analysed HD-ZIP III mutants and S.B. carried out RNA in situ hybridization and lineage tracing with 6-benzylaminopurine. M.-F.W. and J.W.R. generated and tested the amiMP plasmid. A.S.-G. and M.L.G. provided data on the inducible miR165a line. A.A. conducted the statistical analyses. R.S., S.M., P.R. and T.B. provided transgenic lines for the study. O.S. and A.P.M. wrote the manuscript with the help of co-authors.

Competing interests The authors declare no competing interests.

Additional information

Extended data is available for this paper at <https://doi.org/10.1038/s41586-018-0837-0>.

Supplementary information is available for this paper at <https://doi.org/10.1038/s41586-018-0837-0>.

Reprints and permissions information is available at <http://www.nature.com/reprints>.

Correspondence and requests for materials should be addressed to A.P.M.

Publisher's note: Springer Nature remains neutral with regard to jurisdictional claims in published maps and institutional affiliations.

METHODS

No statistical methods were used to predetermine sample size. The experiments were not randomized and investigators were not blinded to allocation during experiments and outcome assessment.

Gene accession numbers. Gene accession numbers are as follows: *CYCB1*;1, AT4G37490; *VND6*, AT5G62380; *WOX4*, AT1G46480; *PXY*, AT5G61480; *PEAR1* (also known as *EPM*, *S29* or *Dof2.4*), AT2G37590; *ANT*, AT4G37750; *AtHB8*, AT4G32880; *CNA* (also known as *AtHB15*), AT1G52150; *PHB*, AT2G34710; *PHV*, AT1G30490; *REV*, AT5G60690; *MIR165A*, AT1G01183; *MP*, AT1G19850; *ARF6*, AT1G30330; *ARF7*, AT5G20730; *ARF8*, AT5G37020; *ARF19*, AT1G19220; *APL*, AT1G79430; and *S17*, AT2G22850.

Plant material and cloning. Most of the entry vectors were generated by PCR amplification of the desired DNA sequence with the primers indicated in Supplementary Table 1, and recombination of the purified PCR product into MultiSite Gateway compatible pDONR entry vectors (Supplementary Table 2). The PCR products that were obtained were amplified in two steps (marked with asterisks in Supplementary Table 2), first with gene-specific primers with partial attB overhangs and then with adaptor primers to generate PCR products with full length attB recombination sequences. The dominant version of *cAtHB8* (*AtHB8d*) has a mutation (CCG to CTG) in the last codon of the *miR165a*-recognition sequence, similar to the dominant *REVOLUTA* mutant *rev-10a*³¹. The entry vector p221z-c *AtHB8d*(-stop) was generated by site-directed mutagenesis using p221z-c *AtHB8*(-stop) as a template and primers *AtHB8dF1* and *AtHB8dR1*, using the QuikChange II Site-Directed Mutagenesis Kit (Agilent Technologies). The entry vector p221a-CYCB1;1-Cre was made by PCR amplification of Cre recombinase³² from p221z-CRE1 using the *CreMfeF* and *CreMfeR* primers, and the resulting PCR product was ligated into the unique *MfeI* restriction site of p221a-CycB1-dbox²⁶. MicroRNA against *MONOPTEROS* (*amiMP*) was obtained by PCR-mutagenizing the *MIR167a* precursor sequences (At3g22886)³³ using the following primers: aMIR-MP_1, aMIR-MP_2, aMIR-MP_3 and aMIR-MP_4 (sequences in Supplementary Table 3). *amiMP* was then cloned into pENTR/D_TOPO to create pENT-*AtMIR167a*-MP. To construct *gANT-GFP*, genomic fragment of *ANT* was amplified by using primers *ANT*(-5172) and *ANT*(+2885R), and cloned into pAN19 (a modified pUC18). GFP was inserted into the C terminus of *ANT* coding sequence by using inverse PCR. The resultant *gANT-GFP* fragment was re-cloned into pBIN30 (a modified pBIN19) binary vector. pSm43GW was generated from pHm43GW in two steps. First, hygromycin resistance was replaced with a -*SphI*-YFP-Kpn1-PCR fragment using the *YFPfrg_F1* and *YFPfrg_R2* primers and the *SphI* and *KpnI* restriction sites to obtain pYm43GW. Next, the YFP fragment was replaced with the sulfadiazine-resistance gene amplified from GABI_874H08 line gDNA with primers *sulf-KpnIF* and *sulf-SnaBIR*, and the resulting PCR product was cloned into pYm43GW using the *KpnI* and *StuI* restriction sites.

MultiSite Gateway technology (Invitrogen) was used to combine promoter (1st box), gene of interest (2nd box) and tag or terminator (3rd box) Gateway entry clones with Gateway-compatible binary destination vectors^{12,34} in a MultiSite LR Clonase reaction. All expression vectors generated in this study are listed in Supplementary Table 4.

All constructs were dipped into the Col-0 ecotype, and single insertion lines were screened based on Mendelian segregation of a selection marker. Several lines for each newly made construct were used for phenotype observation. Plant material produced in this study as well as published lines provided by others are indicated in Supplementary Table 5. The following transgenic and mutant lines have been described elsewhere: *cna-2 phb-13 phv-11*, *athb8-11 cna-2 phb-13 phv-11*^{8,35}, *arf7-1 arf19-1*³⁶, *DR5rev::YFPnuc*³⁷, *DR5rev:erGFP*³⁸, *DR5v2:n3GFP*³⁹, *DR5rev:GUS*⁴⁰, *pWOX4:erYFP*⁴¹, *pMP:MP-GUS*⁴², *pARF7:GUS* and *pARF19:GUS*⁴³, *gARF8-GUS* and *gARF6-GUS*³³, *pG1090:XVE >> axr3-1-RFP*²⁶, *pAPL:GUS*⁴⁴, *gVND6-GUS*⁴⁵ and *pAtHB8:GUS*⁴⁶.

Plant growth and chemical treatments. For almost all experiments, seeds were surface-sterilized in 70% ethanol, then in 20% chlorine, washed twice in H₂O and plated on half-strength GM medium (1/2 GM) containing 0.5 × MS salt mixture with vitamins (Duchefa), 1% sucrose, 0.5g/l MES pH 5.8 and 0.8% agar and vernalized at 4 °C for 2 days. The age of the seedlings was measured from the moment they were placed in a vertical position in the growth cabinet, in which they were grown at 22 °C under long-day conditions. For experiments with soil-grown plants, seeds were directly placed on soil and grown under the same conditions.

17- β -oestradiol (Sigma), a synthetic derivative of oestrogen, and 6-benzylaminopurine (BAP; Sigma)—a cytokinin—were prepared as 20 mM stock solutions in DMSO and stored at -20 °C. EdU, a thymidine analogue (Thermo Fisher), was prepared as a 10 mM stock solution in DMSO and stored at 4 °C. XVE-based gene induction ('Ind' in figure panels) was carried out by transferring plants to plates supplemented with 5 μ M 17- β -oestradiol or an equal volume of DMSO ('mock' in figure panels) unless otherwise indicated. The working concentration of BAP was 0.1 μ M. For EdU treatment, plants were transferred into 1/2 GM liquid medium supplemented with 10 μ M EdU and, eventually, with inducer or mock for 16 h.

Unless stated otherwise, the age of the seedlings at the start of the treatment is indicated in parentheses in the figure legends.

GUS staining, microtome sectioning and histology. GUS detection and histology analysis were performed as previously described⁴⁷, with slight modifications. First, samples were vacuum-infiltrated with the GUS staining solution for 1 h and then incubated at 37 °C until the desired level of GUS staining was obtained (from 2 h to overnight). Samples were cut on a microtome in 10- μ m sections from 5 mm below the root-hypocotyl junction. For histological analysis of clones, the upper 1–1.5-cm root segment was cut every 200 μ m to avoid repeated analysis of the same cells. Finally, root sections were stained for 5 s in a 0.05% (w/v) ruthenium red solution (Fluka Biochemika) or a 0.05% (w/v) toluidine blue solution in deionized water. To stain phloem companion cells, a 0.5% (w/v) safranin solution in 50% ethanol and a 1% (w/v) Alcian blue aqueous solution were used. All histological stainings used in each figure are indicated in Supplementary Table 6.

Fluorescent marker analysis, vibratome sectioning and EdU detection. To analyse fluorescent reporters from a lateral view, roots were fixed in 4% paraformaldehyde (PFA, Sigma) in 1 × PBS pH 7.2 overnight, washed twice in 1 × PBS and cleared in ClearSee solution⁴⁸ supplemented with 1 μ g/ml calcofluor white (Sigma) for at least three days.

Vibratome sectioning was used for fluorescent marker analysis and EdU detection. Roots were fixed in 4% PFA in 1 × PBS pH 7.2 for 1 h under vacuum, washed in ice-cold 1 × PBS and embedded in 4% agarose in 1 × PBS. Samples were cut on a vibratome in 200- μ m sections from 5 mm below the root-hypocotyl junction. Agarose slices that were obtained that contained root cross-sections were washed twice in 1 × PBS, cell walls were stained with 1 μ g/ml calcofluor white (Sigma) in 1 × PBS for between 3 h and overnight and finally cleared with ClearSee solution. To visualize EdU-positive nuclei with the Click-iT EdU Alexa Fluor 488 Imaging Kit (Thermo Fisher), fixed cross-sections were washed twice in 1 × PBS and then incubated in a modified EdU detection cocktail⁴⁹ at room temperature for 1 h, washed twice in 1 × PBS and stained with 1 μ g/ml calcofluor or DAPI solution in 1 × PBS.

Microscopy and image processing. Histological cross-sections were imaged using a Leica 2500 microscope (20 × and 40 × objectives). Confocal analysis was carried out with Leica SP5 and SP8 microscopes. Confocal images were acquired with the Leica LAS AF Software using ClearSee, 1 × PBS or water as an imaging medium. All combinatorial fluorescence analyses were run in sequential scan mode. Confocal settings may have varied between experiments but always remained the same for an experimental sample and the corresponding control. However, to better visualize calcofluor-stained cell walls, the signal was sometimes unevenly adjusted between the sample and the control. EdU images represent maximal projections of five consecutive optical sections captured each 5 μ m in the z-direction.

Microsoft PowerPoint with image compression mode off was used to compile all the figures and to modify brightness and contrast, which was always identically applied to sample and control pictures. Images in Fig. 1a were cropped and rotated using Corel Photo Paint X6, which occasionally resulted in empty corners; for aesthetic reasons, these were filled with a triangle of a similar colour as the image background.

Marker expression quantification, EdU and xylem vessel histograms. Changes in marker expression were analysed from the lateral view; optical sections were captured in the middle of the root, which was determined by the root edges being in focus in the transmitted light channel. The data represent the relative width of the fluorescent domain compared with the root diameter. *DR5:nYFP*, *DR5v2:nGFP* and *cAtHB8-YFP* fluorescence were captured as one stack of 16-bit confocal images from 15 cross-sections. The signal intensities of fluorescent nuclei were measured in ImageJ using multi-point tool with mark width set to 15 pixels. Relative intensities were determined by comparing the signal with the brightest value in the whole dataset. For EdU and vessel distribution histograms, relative distances of EdU nuclei and vessels were determined by comparing their distance from the centre of the xylem axis with the radius of the root. If not indicated otherwise, 25 cross-sections were analysed. Histograms represent frequencies of EdU nuclei or vessels along the radial axes divided into 10 bins in percentage. Distance measurements were done using Leica Lite or ImageJ.

amiMP analysis. Owing to persistent silencing of *pUBQ10:XVE >> amiMP* (*arf7-1 arf19-1*) in the T2 and T3 generations, individual plants were analysed in the T1 generation. Transformants in the *arf7 arf19* or wild-type backgrounds were grown on plates with 20 μ g/ml phosphinothricin (basta, Duchefa) for 5 days without noticeable phenotypes caused by the selection, and then induced together with the controls for 7 days. Segments of the upper 2 cm of the root were collected for histological analysis, and the remaining (lower) part was used for RNA isolation. Because *arf7-1 arf19-1* does not produce lateral roots, the lower segment contained RNA exclusively from the primary root. Cell divisions were counted as the number of cells in one radial cell file between the primary phloem pole and the xylem axis. **qRT-PCR.** RNA was extracted from the top 2 cm of the main root with lateral roots removed using the GeneJET Plant RNA purification kit (Thermo Fisher)

and treated with DNase (Thermo Fisher). cDNA was synthesized from 100 ng (*AtHB8d*- and miR165a-overexpressing plants), 500 ng (*axr3-1*-overexpressing plants and miR165a-overexpressing plants for *PXY*) or 50 ng (amiMP plants) of RNA using MAXIMA H Minus reverse transcriptase (Thermo Fisher) with Oligo(dT) primers (Thermo Fisher). The PCR reaction was done on a Bio-Rad CFX384 cyler using EvaGreen qPCR mix (Solis Biodyne) and the following program: 10 min at 95 °C, 50 cycles (10 s at 95 °C, 10 s at 60 °C, 30 s in 72 °C). All primers used in qRT-PCR are listed in Supplementary Table 6: primers for *ACT2*, *UBQ10* and *ANT*⁵⁰; *PHB*, *PHV*, *AtHB8* and *CNA*⁸; *PXY*⁵¹; and *TIP41*⁵² have previously been described. Results were normalized, following previously published methods^{53,54}, to the reference genes *ACT2*, *UBQ10* and *TIP41*. Three biological replicates were used for each line and time point, as well as three technical replicates, except in the analysis of amiMP lines (see above).

RNA in situ hybridization. Primers used for RNA probe synthesis have previously been published⁸. Sample preparation, sectioning, probe synthesis using T7 RNA polymerase (Thermo Fisher) and hybridization were performed as described⁵⁵ with slight modifications. The uppermost 1-cm segment of the main root was cut from 21-day-old soil-grown plants, and the tissues were vacuum-infiltrated in FAA (50% ethanol; 5% acetic acid; 3.7% formaldehyde) for 30 min and then fixed overnight at 4 °C. For paraffin-embedding, a Leica ASP200 vacuum tissue processor was used, following the protocol indicated in Supplementary Table 7.

Clone induction. To induce clones before the onset of secondary growth, plates with 4-day-old seedlings grown on 1/2 GM plates with or without BAP were heat-shocked at 37 °C for 14 or 17 min, immediately cooled at 4 °C for 15 min and further grown on new 1/2 GM plates under normal growth conditions until GUS staining and histological analysis. For lineage tracing in active cambium, plants were grown for 15 days before heat-shock. Clonal activation of *pUAS:MPΔ-GUS* (Fig. 4a) was carried out in the same way and the clones were analysed 6 days later. For lineage tracing in one-month-old plants, whole 5-cm pots with individual plants were transferred into a 37 °C water bath for 15 min followed by a cooling step under cold tap water for 1 min. Clone activation in the phloem pole pericycle and surrounding cells (S17 domain) was performed by transferring 5-day-old seedlings into liquid 1/2 GM medium with 17-β-oestradiol for 8 or 16 min followed by four 15-min washes in medium without an inducer. After that, plants were placed back on agar plates and grown under normal conditions. *ANT:XVE >> cre* transformants in the *35S:lox-GUS*^{+/+} background were selected on plates with hygromycin and claforan. After four days, hygromycin-resistant plants were transferred on plates with claforan only, and grown further without a noticeable phenotype caused by antibiotics. Clones in the *ANT* domain were induced in a similar way as S17 clones, with slight modifications: 17-day-old plants were incubated with an inducer for 5 or 20 min and, after washing, they were placed on agar plates with claforan. To increase the proportion of clones originating from single cells, roots were pre-screened and only those with a low number of clones were analysed further.

Fate map and lineage-tracing quantification. Because the position of major cell types in the primary root vasculature is invariant, the fate map was generated by counting the frequencies of different GUS sectors and grouping them into three categories: (i) the most frequent basic sectors, (ii) large sectors, which partially share clonal boundaries with two or more basic sector types at once and (iii) half sectors, which consist of a subdomain of one of the basic sector types. Only basic sectors are presented in the fate map (Fig. 1b). BAP-mediated promotion of procambium formation in the place of protoxylem is not a fully penetrant phenotype⁵⁶, and therefore the presence or absence of protoxylem (+) protoxylem or (-) protoxylem, respectively, in Extended Data Fig. 2e, f) was observed before analysing the sectors.

Quantification of GUS sectors in active cambium was carried out by counting the cellular distance of sector boundaries (xylem side ($y < 0$); phloem side ($y > 0$)) from periclinally dividing cambial cells ($y = 0$) in the radial direction. Dividing cambial cells were identified histologically on the basis of the presence of a thin cell wall. In rare cases in which two dividing cambial cells were in a given cell file, the distance was counted from the cell wall between those cells. Only atypically large GUS sectors, sectors with unclear borders or sectors that were located far from the vascular cambium (Extended Data Fig. 5a, b, f) were excluded from quantification. Each bar in graphs (Fig. 1d, Extended Data Fig. 5d, h) represents the size and position of an individual sector; bars with extensions denote sectors beginning or ending with a xylem vessel.

Quantification of *MPΔ* and *VND6* clones. The cell-autonomous effects of *MPΔ* and *VND6* clones on cambial marker-gene induction were measured as the number of independent YFP-positive nuclei that showed marker expression within the clones two days after induction. The cell-non-autonomous effects were quantified as the number of ectopic vessels that showed marker expression in the surrounding cells seven days after induction. At least ten roots per genotype were quantified. The cell-non-autonomous effect of MP on periclinal cell division was analysed by counting the frequency of periclinal cell divisions induced 16 days after germination, in the GUS-negative cells surrounding the *MPΔ-GUS* clones or ectopic vessel.

In these experiments (Fig. 4a, Extended Data Fig. 9e), periclinal cell divisions refer to cell division planes parallel to the surface of the neighbouring *MPΔ*- or *VND6*-induced vessels or clones. Only clearly ectopic vessels or clones (that is, outside the vascular cambium) were analysed further.

General methodology and statistical analysis. Unless otherwise stated, the number of individual plants, root sections or clones analysed is indicated as the n value in figure panels or legends. The fraction given in the corner of some figure panels denotes the frequency of the presented phenotype. Statistical analyses were all carried out in R version 3.5.0 (<http://www.r-project.org/>). For the mean comparison analysis, first the Shapiro–Wilk test for normality was performed and—upon failing to reject or rejecting this hypothesis—the appropriate one- or two-sided Student t -test, or the nonparametric Wilcoxon rank sum test, was performed, respectively. Regression analyses were performed following the affirmation of the normality assumption of the residuals. In general, we considered 0.05 as the significance threshold for P values. The Kullback–Leibler divergent distance was used to quantify the level of dissimilarity between histograms, and finally, the mean between the two directional values is reported. For all box plots, the centre line represents the median and the lower and upper limits of boxes indicates the 25th and 75th percentiles, respectively. Whiskers show the maximum or minimum values, and empty and filled circles represent the individual samples and outliers, respectively.

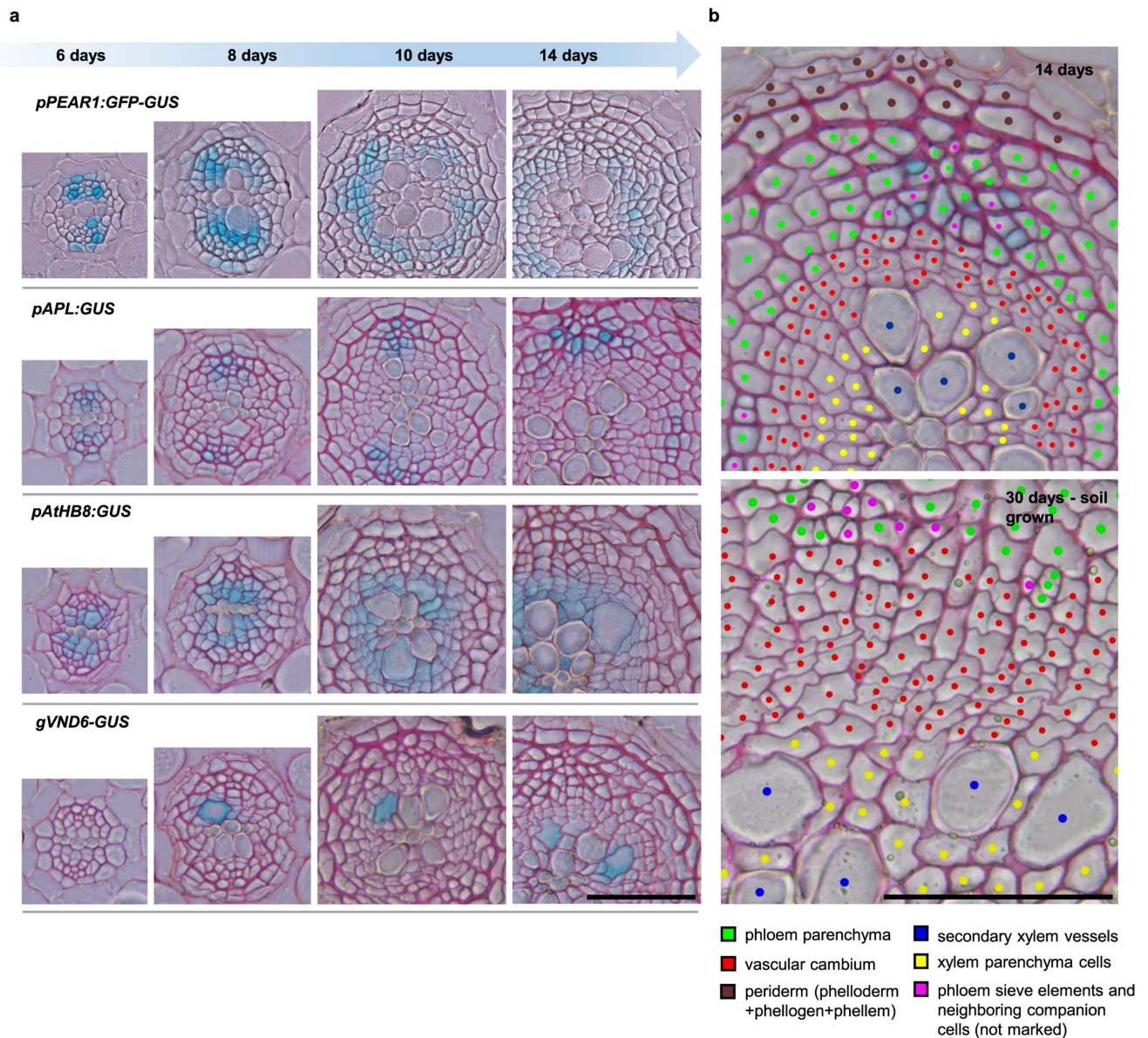
Reporting summary. Further information on research design is available in the Nature Research Reporting Summary linked to this paper.

Data availability

Gene accession numbers of all the *Arabidopsis* genes analysed in this study are listed above. Source Data related to Fig. 2b, c, 3a, b, d and Extended Data Figs. 3d, 4a, c, d, 6a–e, 7b, f, g, 8a–e, 9f are provided with the paper. All lines and other data supporting the findings of this study are available from the corresponding author upon request.

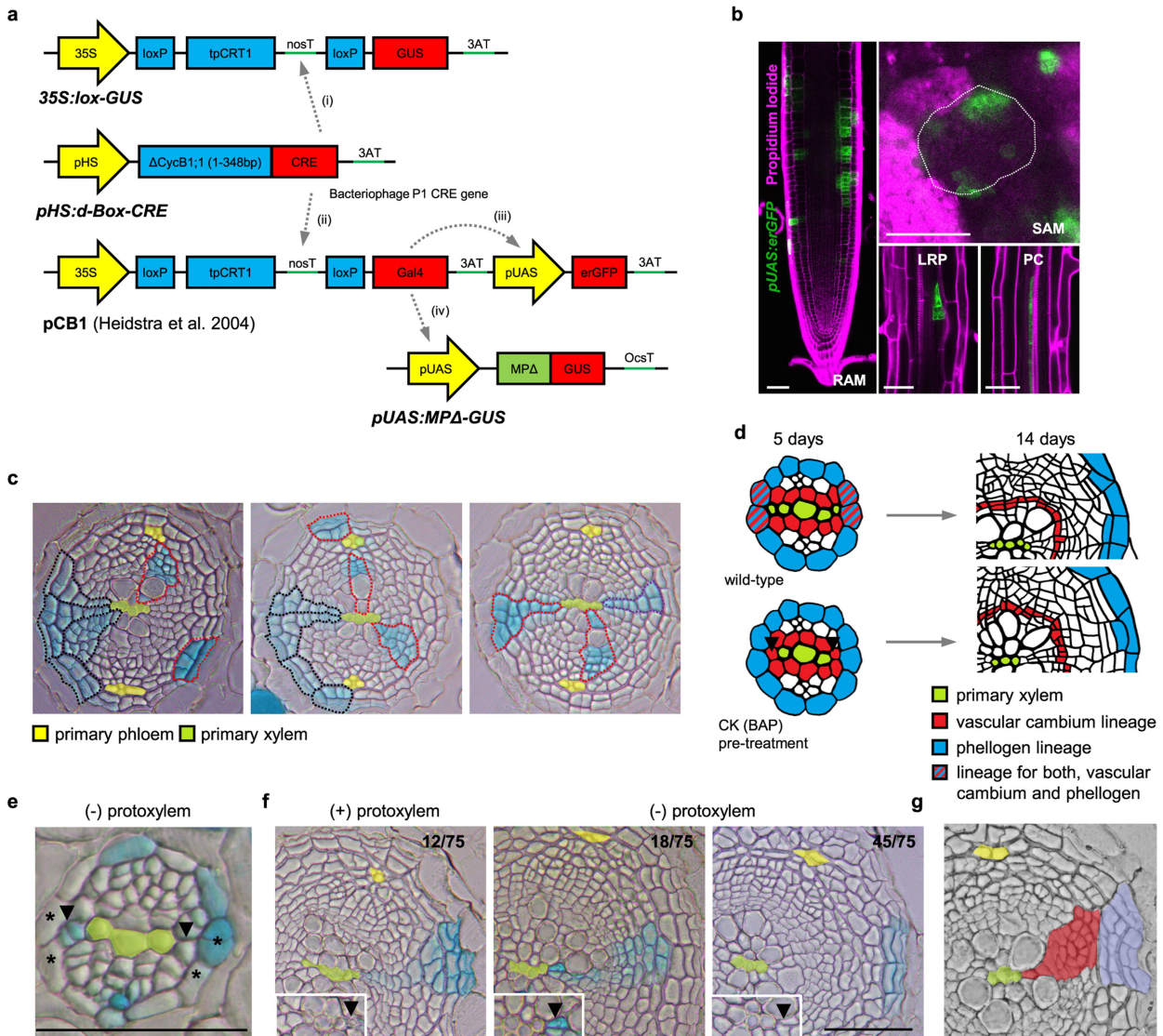
- Emery, J. F. et al. Radial patterning of *Arabidopsis* shoots by class III HD-ZIP and KANADI genes. *Curr. Biol.* **13**, 1768–1774 (2003).
- Heidstra, R., Welch, D. & Scheres, B. Mosaic analyses using marked activation and deletion clones dissect *Arabidopsis* SCARECROW action in asymmetric cell division. *Genes Dev.* **18**, 1964–1969 (2004).
- Wu, M. F., Tian, Q. & Reed, J. W. *Arabidopsis microRNA167* controls patterns of *ARF6* and *ARF8* expression, and regulates both female and male reproduction. *Development* **133**, 4211–4218 (2006).
- Karimi, M., Depicker, A. & Hilson, P. Recombinational cloning with plant gateway vectors. *Plant Physiol.* **145**, 1144–1154 (2007).
- Prigge, M. J. et al. Class III homeodomain-leucine zipper gene family members have overlapping, antagonistic, and distinct roles in *Arabidopsis* development. *Plant Cell* **17**, 61–76 (2005).
- Okushima, Y. et al. Functional genomic analysis of the *AUXIN RESPONSE FACTOR* gene family members in *Arabidopsis thaliana*: unique and overlapping functions of *ARF7* and *ARF19*. *Plant Cell* **17**, 444–463 (2005).
- Sawchuk, M. G., Edgar, A. & Scarpella, E. Patterning of leaf vein networks by convergent auxin transport pathways. *PLoS Genet.* **9**, e1003294 (2013).
- Friml, J. et al. Efflux-dependent auxin gradients establish the apical–basal axis of *Arabidopsis*. *Nature* **426**, 147–153 (2003).
- Liao, C. Y. et al. Reporters for sensitive and quantitative measurement of auxin response. *Nat. Methods* **12**, 207–210 (2015).
- Baesso, B. et al. Transcription factors PRE3 and WOX11 are involved in the formation of new lateral roots from secondary growth taproot in *A. thaliana*. *Plant Biol.* **20**, 426–432 (2018).
- Suer, S., Agusti, J., Sanchez, P., Schwarz, M. & Greb, T. WOX4 imparts auxin responsiveness to cambium cells in *Arabidopsis*. *Plant Cell* **23**, 3247–3259 (2011).
- Vidaurre, D. P., Ploense, S., Krogan, N. T. & Berleth, T. AMP1 and MP antagonistically regulate embryo and meristem development in *Arabidopsis*. *Development* **134**, 2561–2567 (2007).
- Wilmoth, J. C. et al. NPH4/ARF7 and ARF19 promote leaf expansion and auxin-induced lateral root formation. *Plant J.* **43**, 118–130 (2005).
- Bonke, M., Thitamadee, S., Mähönen, A. P., Hauser, M. T. & Helariutta, Y. APL regulates vascular tissue identity in *Arabidopsis*. *Nature* **426**, 181–186 (2003).
- Zhong, R., Lee, C., Zhou, J., McCarthy, R. L. & Ye, Z. H. A battery of transcription factors involved in the regulation of secondary cell wall biosynthesis in *Arabidopsis*. *Plant Cell* **20**, 2763–2782 (2008).
- Baima, S. et al. The expression of the *Atbb-8* homeobox gene is restricted to provascular cells in *Arabidopsis thaliana*. *Development* **121**, 4171–4182 (1995).
- Idänheimo, N. et al. The *Arabidopsis thaliana* cysteine-rich receptor-like kinases CRK6 and CRK7 protect against apoplastic oxidative stress. *Biochem. Biophys. Res. Commun.* **445**, 457–462 (2014).
- Kurihara, D., Mizuta, Y., Sato, Y. & Higashiyama, T. ClearSee: a rapid optical clearing reagent for whole-plant fluorescence imaging. *Development* **142**, 4168–4179 (2015).
- Kotogany, E., Dudits, D., Horvath, G. V. & Ayaydin, F. A rapid and robust assay for detection of S-phase cell cycle progression in plant cells and tissues by using ethynyl deoxyuridine. *Plant. Methods* **6**, 5 (2010).

50. Randall, R. S. et al. *AINTEGUMENTA* and the D-type cyclin *CYCD3;1* regulate root secondary growth and respond to cytokinins. *Biol. Open* **4**, 1229–1236 (2015).
51. Liebsch, D. et al. Class I KNOX transcription factors promote differentiation of cambial derivatives into xylem fibers in the *Arabidopsis* hypocotyl. *Development* **141**, 4311–4319 (2014).
52. Czechowski, T., Stitt, M., Altmann, T., Udvardi, M. K. & Scheible, W. R. Genome-wide identification and testing of superior reference genes for transcript normalization in *Arabidopsis*. *Plant Physiol.* **139**, 5–17 (2005).
53. Vandesompele, J. et al. Accurate normalization of real-time quantitative RT-PCR data by geometric averaging of multiple internal control genes. *Genome Biol.* **3**, RESEARCH0034 (2002).
54. Livak, K. J. & Schmittgen, T. D. Analysis of relative gene expression data using real-time quantitative PCR and the $2^{-\Delta\Delta C_t}$ method. *Methods* **25**, 402–408 (2001).
55. Yang, W., Wightman, R. & Meyerowitz, E. M. Cell cycle control by nuclear sequestration of *CDC20* and *CDH1* mRNA in plant stem cells. *Mol. Cell* **68**, 1108–1119 (2017).
56. Mähönen, A. P. et al. Cytokinin signaling and its inhibitor AHP6 regulate cell fate during vascular development. *Science* **311**, 94–98 (2006).
57. Colón-Carmona, A., You, R., Haimovitch-Gal, T. & Doerner, P. Technical advance: spatio-temporal analysis of mitotic activity with a labile cyclin–GUS fusion protein. *Plant J.* **20**, 503–508 (1999).
58. Bishopp, A. et al. A mutually inhibitory interaction between auxin and cytokinin specifies vascular pattern in roots. *Curr. Biol.* **21**, 917–926 (2011).
59. De Rybel, B. et al. Integration of growth and patterning during vascular tissue formation in *Arabidopsis*. *Science* **345**, 1255–1258 (2014).
60. Ohashi-Ito, K. et al. A bHLH complex activates vascular cell division via cytokinin action in root apical meristem. *Curr. Biol.* **24**, 2053–2058 (2014).
61. Matsumoto-Kitano, M. et al. Cytokinins are central regulators of cambial activity. *Proc. Natl Acad. Sci. USA* **105**, 20027–20031 (2008).



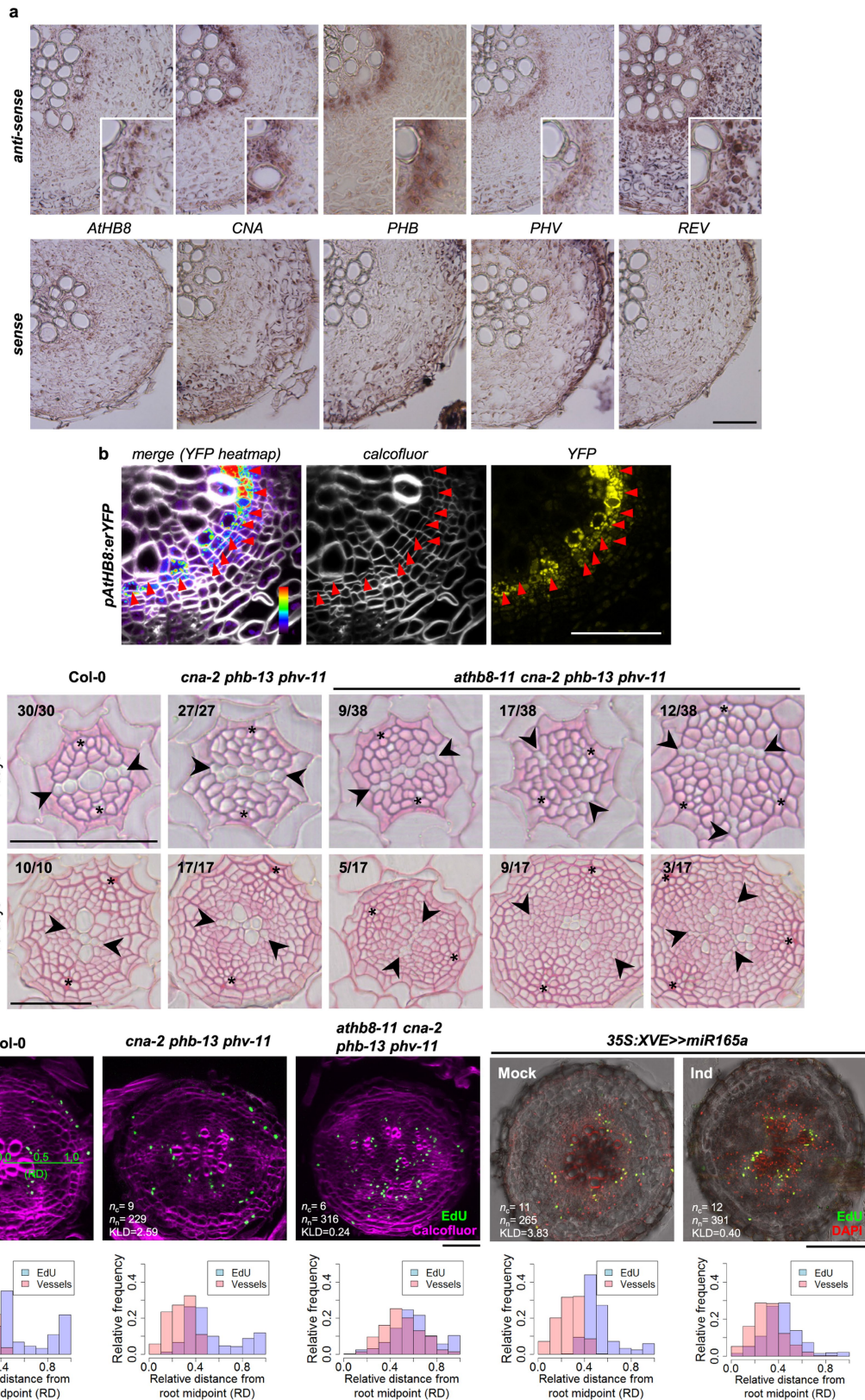
Extended Data Fig. 1 | Ontogeny of different cell types after activation of secondary growth in *Arabidopsis* root. **a**, Bright-field microscopy of root cross-sections of an early phloem marker (*PEAR1*), a marker of differentiating phloem expressed in phloem-companion cells (*APL*), an early xylem marker (*AtHB8*) and a marker specific to differentiating xylem vessels (*VND6*) at different times after secondary growth activation. **b**, Histological analysis of different cell types found in 14-day-old root that expresses a phloem differentiation marker *pAPL:GUS* (top) and in 30-day-old wild-type root (bottom). Cambium (red) typically consists of 2–4 cells

(14-day-old root) or 7–9 cells (30-day-old root). It is located between fully differentiated phloem elements (purple) and xylem vessels (blue), and is characterized by frequent cell divisions, detected histologically as a recently made thin cell wall. Xylem- and phloem-parenchyma cells are quiescent cells located between xylem vessels, or rarely dividing cells located between differentiated phloem cells, respectively. Data shown are representative of at least three independent experiments. Scale bars, 50 μm .



Extended Data Fig. 2 | A lineage-tracing tool for developmental studies in plants. **a**, A schematic of two clonal activation systems. Cre recombinase was fused to the N-terminal part of *CYC1;1*⁵⁷ to make *CYC1;1-Cre* stable only in meristematic cells that are transiting between the early G2 and M phases of the cell cycle. Heat-shock induction of *pHS:CYC1;1-cre* causes recombination of two loxP sites, which activates expression of *35S:GUS* (labelled (i)) or *35S:GAL4* (labelled (ii)), respectively. In the second step, the *35S:GAL4* transactivates *pUAS:erGFP* (labelled (iii)) and—if desired—another gene of interest cloned under *pUAS* in a third construct (labelled (iv)). **b**, Confocal microscopy of the root (RAM) and shoot (SAM; dashed line, top view) apical meristems, lateral root primordium (LRP) and procambium (PC) containing GFP clones 15 h after induction, in 5-day-old seedlings containing *pHS:CYC1;1-cre* and *pCB1*³² constructs. Because of the instability provided by the *CYC1;1-Cre* fusion and the apparent non-synchronicity of the cell cycle, a high frequency of single-cell-descent clones was obtained almost exclusively in the dividing cells in the apical and lateral meristems. **c**, Examples of the three different GUS sector categories: basic sectors originate from a single-cell clone induced before the activation of secondary growth (red, 75%), large sectors originate from a cluster of clones simultaneously induced in several neighbouring cells (black, 19%),

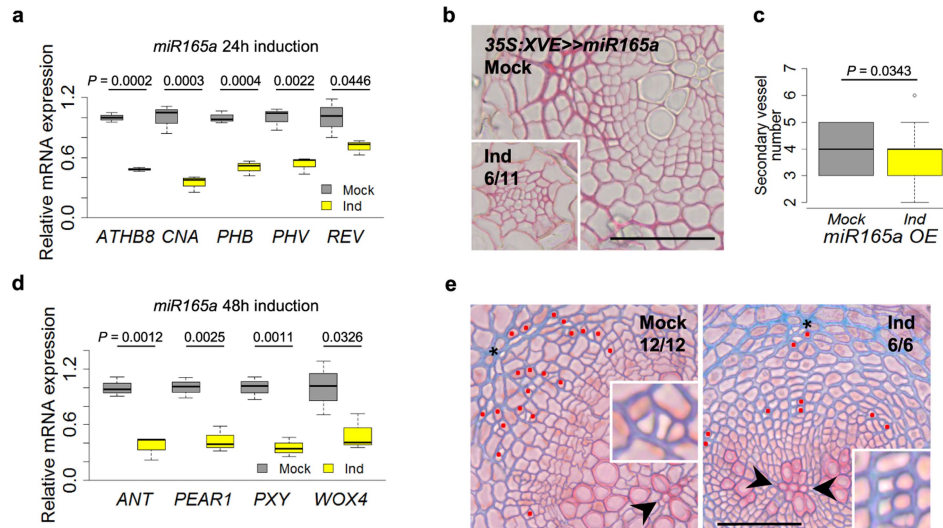
and half sectors originate from a single-cell clone induced after the activation of secondary growth (purple, 6%). A total of 176 sectors was analysed. **d**, A schematic of vascular cambium (red) and phellogen (blue) ontogeny. Under normal conditions (top) both meristems originate from XPP cells. When roots are pre-treated with cytokinin (CK), cells in the protoxylem position (black arrowheads) remain procambial cells⁵⁶, and are thus capable of contributing to secondary growth (bottom, CK). In these experimental conditions, separation of vascular cambium and phellogen lineages has already occurred during primary growth, and connection with the xylem remains the determining factor for the origin of vascular cambium. **e**, Examples of GUS clones 24 h after heat-shock in cytokinin (BAP) pre-treated roots. Arrowheads, procambial cells in place of protoxylem; asterisks, pericycle cells that have lost their xylem connection. **f**, Correlation of different shapes of the GUS sector with the presence (left) or absence (centre, right) of protoxylem (insets, arrowheads). The numbers represent the frequency of these sectors. **g**, XPP-cell fate map of roots pre-treated with BAP. XPP cells that lose their xylem connection behave similar to pericycle cells (light purple, compare with Fig. 1b); cells in the protoxylem position behave similar to xylem-procambial cells, making wide sectors (red, compare with Fig. 1b). In **b**, **e**, **f**, experiments were repeated at least two times with similar results. Scale bars, 50 μ m.



Extended Data Fig. 3 | See next page for caption.

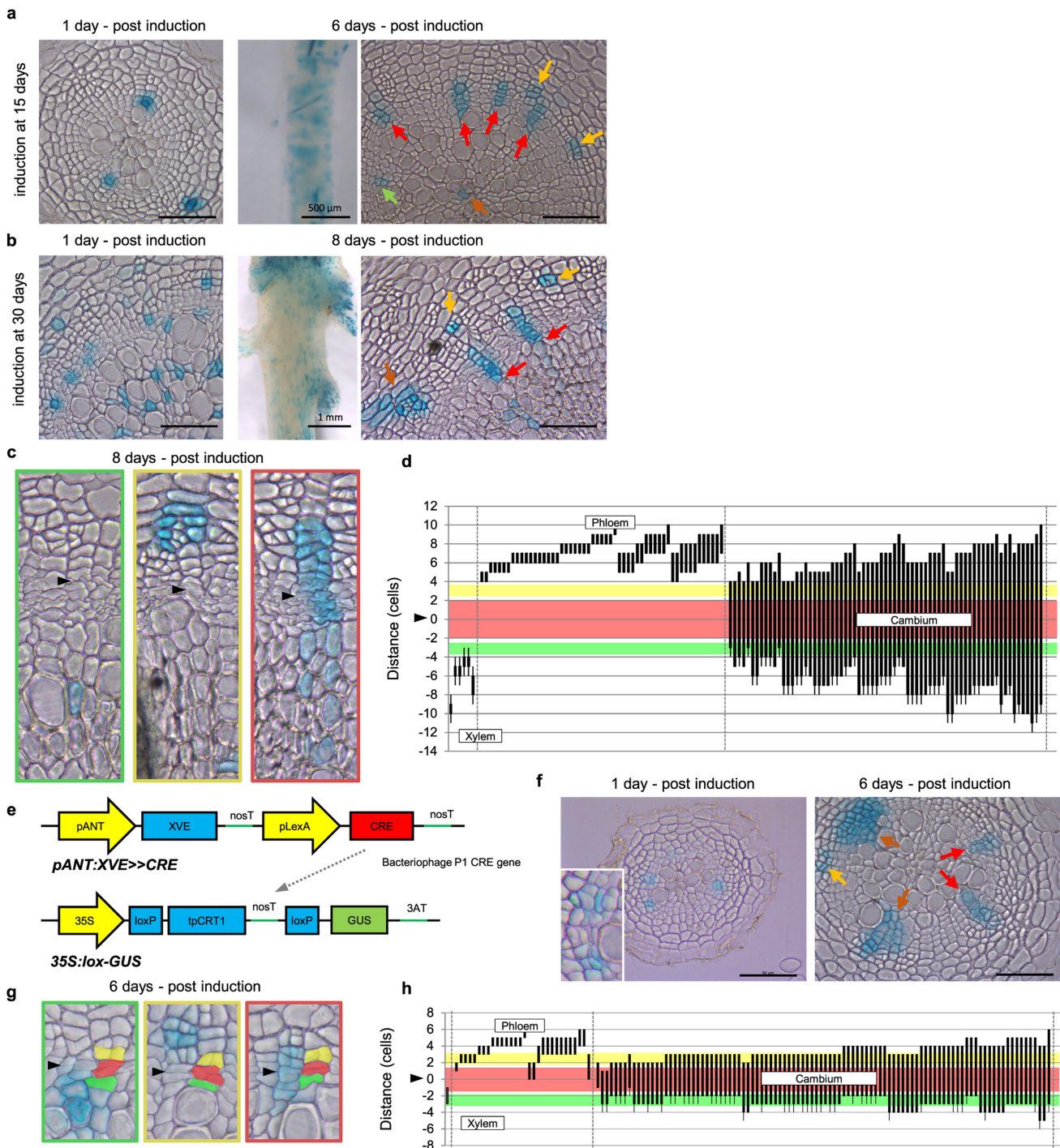
Extended Data Fig. 3 | Transcriptional and mutant analyses of HD-ZIP III transcription factors. **a**, In situ RNA hybridization of sense- and anti-sense probes in cross-sections of 21-day-old, Col-0 plants, showing expression of HD-ZIP III transcription factors in the cambium. Insets are $2\times$ magnifications of the cambial region of the same photograph. **b**, Confocal microscopy of root cross section of 14-day-old *pAtHB8:erYFP* plants. Cell wall staining in grey. Red arrowheads, recent cell divisions in cambium. **c**, Bright-field microscopy of primary and secondary vasculature shows patterning defects in higher-order HD-ZIP III mutants 7 days and 10 days after germination. Col-0 and *cna-2 phb-13 phv-11* show normal differentiation of the primary xylem axis and two phloem poles, whereas the majority of *athb8-11 cna-2 phb-13 phv-11* roots did not have a fully differentiated xylem axis, or showed a triarch pattern with three phloem poles. The fraction in top left corner denotes the frequency of the presented phenotype. Asterisks, primary phloem poles; arrowheads, extremities of the primary xylem. **d**, Confocal images of

EdU-stained (green) nuclei in *cna-2 phb-13 phv-1* and *athb8-11 cna-2 phb-13 phv-11* mutants and the miR165a overexpressor (top). miR165a was induced for 12 days (starting from 4-day-old plants), and the mutants were 14 days old. Inhibition of HD-ZIP III transcription factors leads to cambium disorganization (histograms, bottom). Even though *AtHB8*, *CNA*, *PHB* and *PHV*—and perhaps also *REV*—are redundantly required for secondary xylem formation and normal cambium organization, it is possible that individual members of the family have distinct function in the cambial stem cells and their organizers. Histograms of the relative distances (RD) of EdU-positive nuclei and secondary xylem vessels in the radial direction from the root midpoint (xylem axis, $x = 0$; root surface, $x = 1$, with the scale shown in green in the Col-0 panel). KLD indicates the mean Kullback–Leibler distances between EdU-positive nuclei and vessels. n_c = number of cross-sections analysed; n_n = total number of nuclei. In **a** and **b**, data shown are representative of two (**a**) or four (**b**) independent experiments. Scale bars, 50 μm .



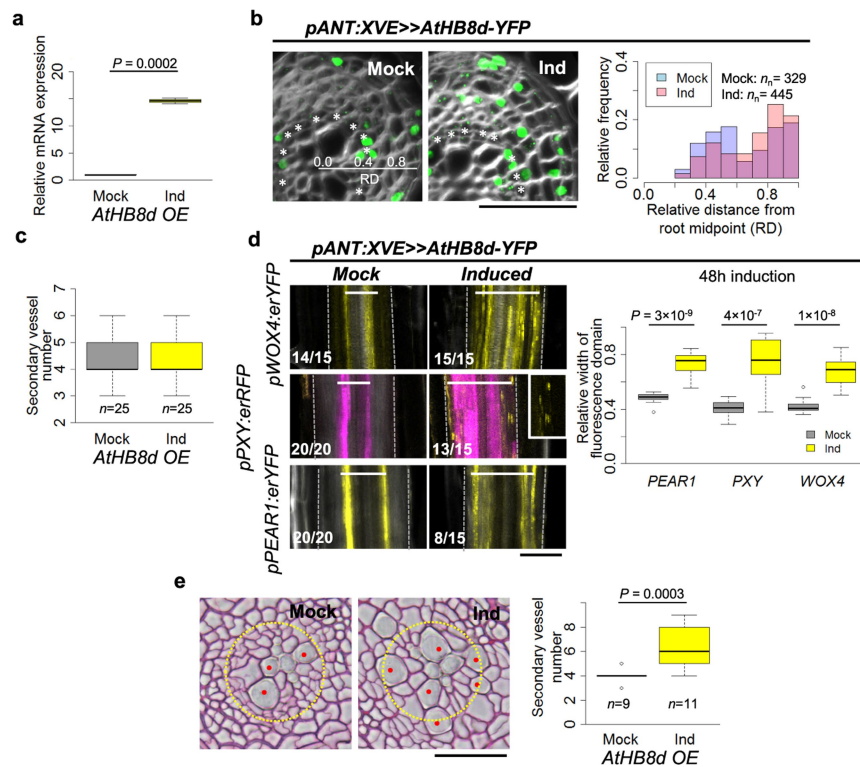
Extended Data Fig. 4 | Phenotypic characterization of inducible miR165a line. **a**, qRT-PCR analysis of transcription of HD-ZIP III transcription factors after miR165a induction for 24 h (in 9-day-old plants). **b**, miR165a-overexpressing plants grown on induction medium for 14 days (from germination onwards) resemble the quintuple HD-ZIP III mutant⁸. **c**, Quantification of secondary xylem vessel formation after miR165a induction for 2 days (in 8-day-old plants). Phenotypic changes on secondary vessel number start to appear within two days of the induction. A two-tailed Wilcoxon test ($n = 25$ independent roots). **d**, qRT-PCR analysis for marker-gene expression after a 2-day *miR165a*

induction (in 8-day-old plants). **e**, Bright-field microscopy of miR165a overexpressor, double stained with Safranin and Alcian blue to highlight secondary phloem (insets) after miR165a induction for 12 days (starting from 4-day-old plants). Red dots, secondary phloem; asterisk, primary phloem; arrowheads, extremities of the primary xylem. *P* values in **a** and **d** are from a one-tailed *t*-test. Data are from three experiments ($n = 10$ roots per treatment). In **b** and **e**, the fraction denotes the frequency of the presented phenotype. Box-and-whisker plots show median and interquartile range; whiskers show range, and dots show outliers. Scale bars, 50 μ m.



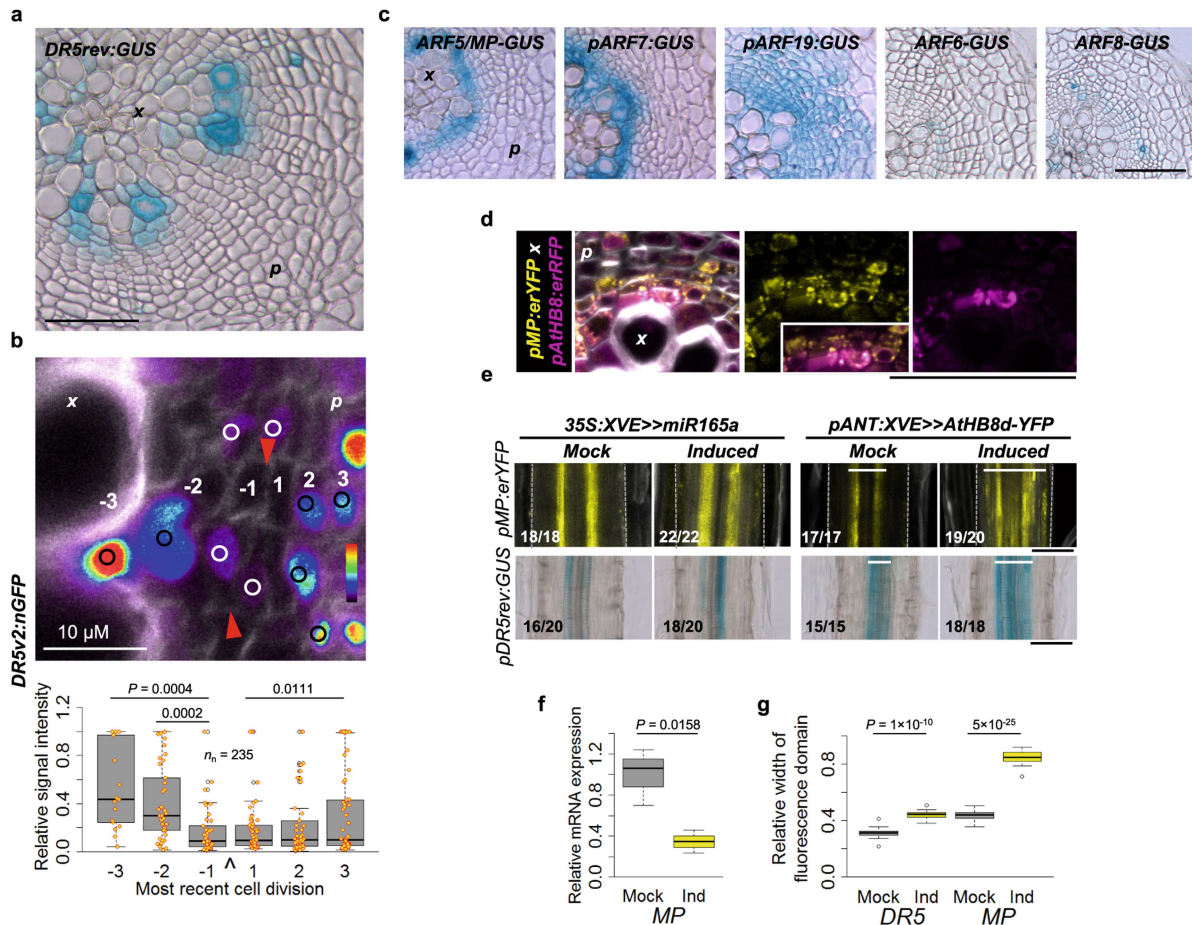
Extended Data Fig. 5 | Lineage tracing in active cambium using two different lineage-tracing systems. a–d, GUS sectors obtained after clone induction in 15-day-old (**a**) and 30-day-old (**b–d**) plants harbouring *pHS:d-Box-cre* and *35S:lox-GUS* constructs (see Extended Data Fig. 2a). **a, b,** Middle panels are lateral view of roots with GUS sectors before sectioning. **c, d,** Lineage tracing in 30-day-old cambium revealed that bifacial stem cells are present, even in wide cambium in which 7–9-cell layers could be identified histologically (see Extended Data Fig. 1b). Quantification was performed as in Fig. 1d. **e–h,** Lineage tracing in *ANT*-expression domain. **e,** A schematic of clonal activation system used to induce GUS clones in the *ANT*-expression domain. After induction, *cre*-directed recombination leads to clonal activation of the GUS reporter. **f,** GUS sectors obtained after clone induction in 17-day-old plants containing *pANT:XVE >> cre* and *35S:lox-GUS*. Inset is a 2.5× magnification of the cambial zone of the same image. **g, h,** Lineage tracing

in active cambium showed *ANT* as a stem-cell marker. Six days after induction (in 17-day-old plants), growing GUS sectors had either a xylem (green) or phloem (yellow) fate but the majority (76%) had a cambial fate (red), on the basis of the position of thinnest cell wall (arrow) in radial direction (which represents the most recent periclinal cell division in cambium) ($y = 0$). **d, h,** Each bar represents the size and position of an individual sector ($n = 131$); bars with extensions denote sectors beginning or ending with a xylem vessel. **a, b, f,** Red arrows, sectors originating from cambium stem cells; yellow arrow, sectors on the phloem side; green arrow, sectors on the xylem side; brown arrow, examples of sectors excluded from the quantification analysis. GUS staining is weak or absent in differentiated xylem vessels. Data represents sectors collected across at least 15 (**a, f–h**) or 4 (**b–d**) independent roots. Experiments were repeated at least twice with similar results. Scale bars, 50 μm (unless otherwise specified).



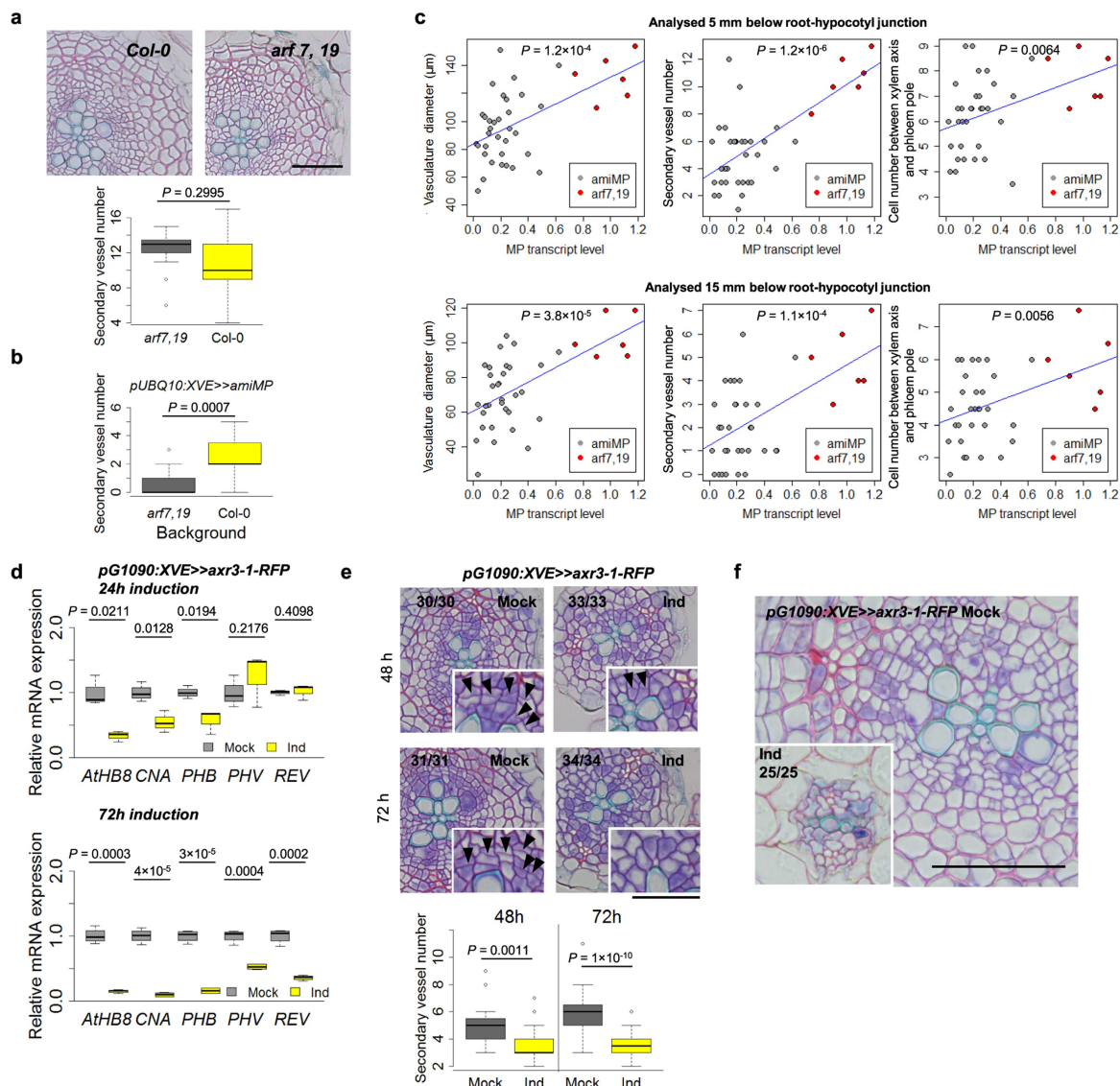
Extended Data Fig. 6 | Phenotypic characterization of inducible *AtHB8d* line. **a**, qRT-PCR analysis of *AtHB8d* expression after *AtHB8d* induction for 24 h (in 9-day-old plants). **b**, Confocal microscopy of roots after EdU staining of S-phase nuclei reveal a centrifugal shift of the cell division domain after a 2-day *AtHB8d* induction (in 8-day-old plants). Asterisks mark cambium. Histograms showing the relative distances of EdU-positive nuclei in the radial direction from the root midpoint (xylem axis, $x = 0$, root surface, $x = 1$), as depicted in mock. n_n , total number of nuclei. **c**, Quantification of secondary xylem vessel formation after *AtHB8d* induction for 2 days (in 8-day-old plants). **d**, Confocal microscopy of fluorescent markers after a 2-day *AtHB8d* induction

(in 8-day-old plants). Cell wall staining in grey. Dashed lines, borders of the secondary tissues seen from the lateral view. Graph is quantification of the relative width of marker expression domains. **e**, Bright-field microscopy of roots after *AtHB8d* induction for 4 days (in 8-day-old plants) and quantification of secondary xylem vessel numbers. Red dots, secondary xylem vessels; yellow dashed line, cambium position in mock-treated roots. **a**, **d**, One-tailed *t*-test. Data are from three experiments (in **a**, $n = 10$ roots per treatment; in **d**, $n = 10$ roots per treatment indicated in left panels). **c**, **e**, Two-tailed Wilcoxon test. n , independent roots. Box-and-whisker plots show median and interquartile range; whiskers show range, and dots show outliers. Scale bars, 50 μm .



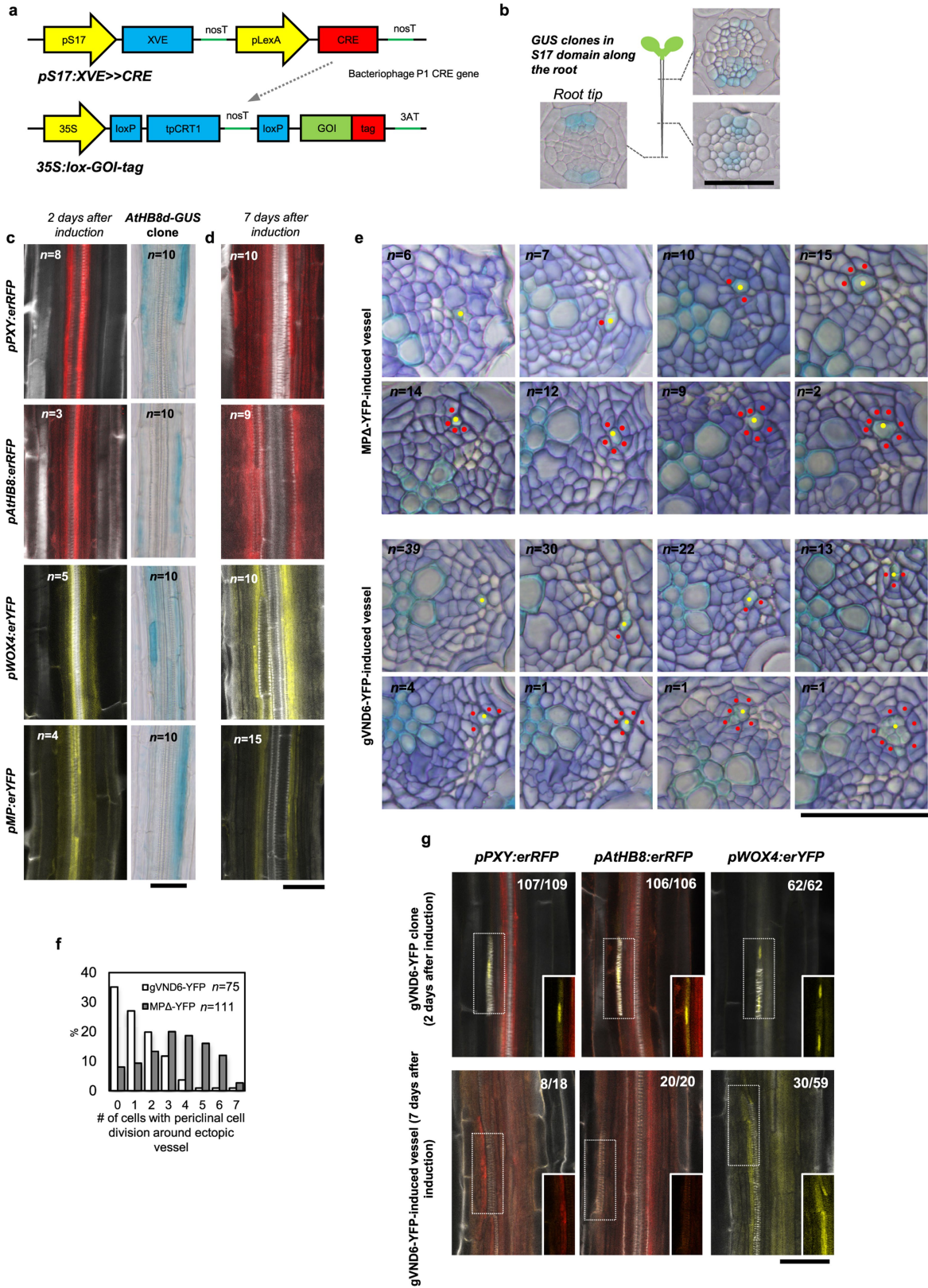
Extended Data Fig. 7 | Auxin signalling and ARF reporters. **a**, Bright-field microscopy of *DR5rev:GUS* root cross-section of a 14-day-old plant. **b**, Confocal microscopy of *DR5v2:nGFP* (heat map) root cross-sections. Nuclear fluorescence signal (examples of regions of interest are indicated with a circle) was quantified in three cell layers from the most recent cell division (arrowheads) towards xylem (positions -1, -2 and -3) and phloem (positions 1, 2 and 3). Fourteen cross-sections were analysed; n_n = total number of nuclei. **c**, Bright-field microscopy of 17-day-old roots expressing class A ARF GUS markers. **d**, Confocal microscopy of 14-day-old plant expressing *pAtHB8:erRFP* and *pMP:erYFP*. **e**, Confocal and bright-field microscopy of *pMP:erYFP* and *DRrev:GUS* marker width after a 2-day *AtHB8d* or *miR165a* induction in 8-day-old plants. Nuclear localization of *AtHB8d-YFP* is shown in Extended Data Fig. 6d. Cell walls in *pMP:erYFP* roots were stained with calcofluor (grey). The

fraction in the bottom left corner denotes the frequency of the presented phenotype. White bars, width of the marker domain. Dashed lines, borders of the secondary tissues. **f**, qRT-PCR analysis of *MP* expression after a 2-day *miR165a* induction in 8-day-old plants. Data are from three experiments ($n = 10$ roots per treatment). **g**, Quantification of the relative width of marker expression domains after *pANT:XVE >> AtHB8d-YFP* induction shown in **e** (right panels). Sample size for each group is equal to denominator of the fraction indicated in **e**. **b**, **f**, **g**, One-tailed *t*-test for the comparison between different positions (**b**) or between mock and induced sample (**f**, **g**). Box-and-whisker plots show median and interquartile range; whiskers show range, and dots show outliers (**g**) or individual data points (**b**). **a**, **c**, **d**, Representative images of at least three independent observations. **b**, **d**, **e**, Cell wall staining in grey. p, phloem; x, xylem. Scale bars, 50 μ m.



Extended Data Fig. 8 | Phenotypic characterization inducible amiMP and *axr3-1* lines. **a**, The *arf7 arf19* double mutant shows no difference in secondary xylem production, when compared to wild-type (*Col-0*) and analysed 14 days after germination, ($n_{Col-0} = 17$ and $n_{arf7 arf19} = 15$ independent roots). **b**, Quantification of secondary xylem vessel formation after amiMP induction for 7 days (in 5-day-old plants) in wild-type ($n_{Col-0} = 7$ independent roots) and *arf7 arf19* ($n_{arf7 arf19} = 34$ independent roots) plants analysed 15 mm below the root-hypocotyl junction. The reduction in xylem vessel formation was less apparent when amiMP was induced in the wild-type background, which indicates that *ARF7* and/or *ARF19* are also required for this process. **c**, Plots of regressions between *MP* transcript levels and vasculature diameter (left), secondary xylem vessel formation (centre) and cell divisions (right) analysed 5 mm (top) and 15 mm (bottom) below the root-hypocotyl junction. Each point represents an individual T1 transformant or *arf7 arf19* plant ($n_{amiMP} = 33$; $n_{arf7 arf19} = 6$) grown for 5 days on a basta selection plate or 1/2 GM and then induced for 7 days. Because the residuals were not normal, a one-way Wilcoxon test for the similarity of the means of the *arf7 arf19* and amiMP groups on *MP* transcription level was performed. A negligible *P* value of

3.065×10^{-7} confirms that the *arf7 arf19* mean is significantly greater than the amiMP mean. To assess the linear relationship between *MP* transcript levels and the observed phenotypes, we performed regression analyses. The plotted blue line indicates the fitted regression model to both groups combined, and the *P* value indicating the goodness of this fit is plotted on the top of each respective graph. **d**, qRT-PCR analysis of the behaviour of HD-ZIP III transcription factors after a 24-h and 72-h induction of *axr3-1* (in 8-day-old plants). Data are from four experiments ($n = 16$ roots per treatment). **e**, Bright-field microscopy and secondary xylem vessel quantification (bottom) of roots after *axr3-1* induction for 48 and 72 h (in 8-day-old plants). Insets are $1.5 \times$ magnifications of the cambial region of the same photo. Arrowhead, recent cell division. Sample size for each group is equal to denominator of the fraction indicated in top panels. **f**, Bright-field microscopy of roots after *axr3-1* induction for 7 days (starting from 5-day-old plants). Box-and-whisker plots show median and interquartile range; whiskers show range, and dots show outliers. **a**, **b**, Two-tailed Wilcoxon test. **d**, **e**, One-tailed *t*-test. In **e**, **f**, the fraction in top left corner denotes the frequency of the presented phenotype. In **a**–**c**, *arf7, 19* refers to *arf7 arf19*. Scale bars, 50 μm .

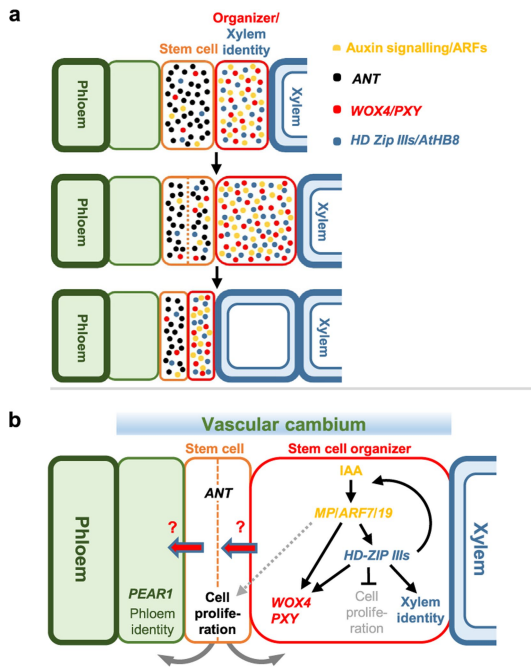


Extended Data Fig. 9 | See next page for caption.

Extended Data Fig. 9 | Clonal activation in the S17 expression domain.

a, A schematic of the clonal activation system to induce clones in phloem-pole pericycle cells and surrounding tissue. After induction, Cre-directed recombination leads to clonal activation of GUS or the gene-of-interest (GOI) (*AtHB8d*, *MPΔ*, or *gVND6*) tagged with a reporter. **b**, Bright-field microscopy of GUS sectors in S17 position analysed 1 day after clone induction (in 5-day-old plants). Induction of large sectors (consisting of several single-cell GUS clones in the root-tip region) recapitulated the previously described expression pattern of the S17 promoter, as being specific to phloem-pole pericycle cells¹⁶ (bottom left). Higher up in the root—where secondary growth has already started—GUS clones were obtained in primary phloem and surrounding tissue (right panels), which suggests that after secondary growth activation the S17 expression domain enlarges centripetally. The experiment was repeated twice with similar results. **c**, **d**, None of 21 *35S:lox-cATHB8d-GUS* transformants in *pS17:XVE >> cre* background showed ectopic vessel formation. **c**, Confocal (left) and bright-field microscopy (right) analysis of *AtHB8-GUS* clones in a cambial marker background. Marker expression was analysed 2 days after clone induction (in 5-day-old plants). The bright-field and confocal

images are from different roots. *n* = number of entire roots screened for ectopic marker expression. **d**, Confocal analysis of *AtHB8d-GUS* clonal activation lines performed 7 days after *AtHB8d-GUS* clone induction (in 5-day-old plants), with calcofluor staining in grey. *n* = number of entire independent roots screened for ectopic vessel formation. **e**, **f**, *MPΔ*- and *gVND6*-induced ectopic vessels show different levels of induction of periclinal cell division in neighbouring cells. Bright-field microscopy of root cross-sections, showing ectopic vessels with periclinal cell division in neighbouring cells analysed 7 days after induction (in 5-day-old plants). Yellow dots, ectopic xylem vessel; red dots, cells that have recently undergone periclinal cell division. *n* = number of xylem vessels examined for each category (0–7 neighbouring cells dividing periclinally). Quantification in **f**. Data were collected across 16 independent roots for each genotype. **g**, Confocal analysis of marker expression within *gVND6-YFP* clones (top) and around *gVND6-YFP*-induced ectopic vessels (bottom). The fraction in top right corner denotes the frequency of the presented phenotype. Cell walls were stained with calcofluor (grey). Insets show merged YFP and RFP channels, except for insets of *WOX4* that show only the YFP channel. Scale bars, 50 μm.



Extended Data Fig. 10 | Model describing the dynamic nature of vascular cambium. **a**, When the organizer cells differentiate into a xylem vessel, a new organizer is formed in adjacent cambial stem cell. Stem cells and their xylem-side daughters dynamically gain organizer-cell gene expression as they mature towards xylem identity. Only the events that lead to xylem production from the bifacial stem cell is unknown, and therefore not presented in the scheme. Density of the dots corresponds to the level of signalling components shown in **b**. **b**, A model presenting a signalling framework that defines the stem-cell organizer of vascular cambium. Question marks refer to unknown factors that promote stem-cell or phloem identity in a non-cell-autonomous manner. These mobile stem-cell-promoting factors could, for example, be cytokinins, which—during primary development—move from primary xylem precursor cells (marked with high levels of auxin signalling) to promote cell division in the neighbouring procambial cells^{58–60}. Supporting this scenario, cytokinins are required for cambial cell proliferation during secondary development⁶¹. Alternatively, WOX4 or other transcription factors expressed in the organizer could move to the adjacent cell to promote stem-cell identity, similar to WUS and WOX5 in the apical meristems².

Reporting Summary

Nature Research wishes to improve the reproducibility of the work that we publish. This form provides structure for consistency and transparency in reporting. For further information on Nature Research policies, see [Authors & Referees](#) and the [Editorial Policy Checklist](#).

Statistical parameters

When statistical analyses are reported, confirm that the following items are present in the relevant location (e.g. figure legend, table legend, main text, or Methods section).

n/a Confirmed

- The exact sample size (n) for each experimental group/condition, given as a discrete number and unit of measurement
- An indication of whether measurements were taken from distinct samples or whether the same sample was measured repeatedly
- The statistical test(s) used AND whether they are one- or two-sided
Only common tests should be described solely by name; describe more complex techniques in the Methods section.
- A description of all covariates tested
- A description of any assumptions or corrections, such as tests of normality and adjustment for multiple comparisons
- A full description of the statistics including central tendency (e.g. means) or other basic estimates (e.g. regression coefficient) AND variation (e.g. standard deviation) or associated estimates of uncertainty (e.g. confidence intervals)
- For null hypothesis testing, the test statistic (e.g. F , t , r) with confidence intervals, effect sizes, degrees of freedom and P value noted
Give P values as exact values whenever suitable.
- For Bayesian analysis, information on the choice of priors and Markov chain Monte Carlo settings
- For hierarchical and complex designs, identification of the appropriate level for tests and full reporting of outcomes
- Estimates of effect sizes (e.g. Cohen's d , Pearson's r), indicating how they were calculated
- Clearly defined error bars
State explicitly what error bars represent (e.g. SD, SE, CI)

Our web collection on [statistics for biologists](#) may be useful.

Software and code

Policy information about [availability of computer code](#)

Data collection

No software was used.

Data analysis

Image J Version 1.47
Microsoft Excel 2013
R version 3.3.2
RStudio 1.1.383
Leica LAS AF Lite 2.6.0.

For manuscripts utilizing custom algorithms or software that are central to the research but not yet described in published literature, software must be made available to editors/reviewers upon request. We strongly encourage code deposition in a community repository (e.g. GitHub). See the Nature Research [guidelines for submitting code & software](#) for further information.

Data

Policy information about [availability of data](#)

All manuscripts must include a [data availability statement](#). This statement should provide the following information, where applicable:

- Accession codes, unique identifiers, or web links for publicly available datasets
- A list of figures that have associated raw data
- A description of any restrictions on data availability

Gene accession numbers of all the Arabidopsis genes analysed in this study are listed in Methods. Source Data related to Fig 2b, c; Fig 3a, b, d; ED Fig 3d; ED Fig 4a, c, d; ED Fig 6a, b, c, d, e; ED Fig 7b, f, g; ED Fig 8a, b, c, d, e; and ED Fig 9f are provided with the paper. All lines and other data supporting the findings of this study are available from the corresponding author upon request.

Field-specific reporting

Please select the best fit for your research. If you are not sure, read the appropriate sections before making your selection.

- Life sciences Behavioural & social sciences Ecological, evolutionary & environmental sciences

For a reference copy of the document with all sections, see [nature.com/authors/policies/ReportingSummary-flat.pdf](https://www.nature.com/authors/policies/ReportingSummary-flat.pdf)

Life sciences study design

All studies must disclose on these points even when the disclosure is negative.

Sample size	Between 7 and 20 plants were analysed for the first experiment. This is comparable to previous studies (Gaudinier et al. 2018 Nature). 3 or 4 biological replicates were used for qRT-PCR experiments and each biological replicate had approximately 10 plants. Except for the amiMP, where individual T1 transformants were used instead.
Data exclusions	We excluded samples that germinated poorly, or showed overall growth defects that were confirmed genetically not to be related to the genotype. These defects occur occasionally, and are caused by the seed sterilization method used.
Replication	Lines which showed statistically significant differences in the initial experiments were analysed further by repeating the experiment at least two more times (except for RNA in situ hybridization, which was carried out twice). Final figures are showing one representative repeat. For qRT-PCR experiments all biological replicates were combined for the final analysis and figure.
Randomization	For each experiment mutant/treated plants and control plants were plated on individual plates and placed in random order into the growth chamber.
Blinding	We did not use blinding. In order to get as objective results as possible, in multiple experiments we had other researchers repeating the experiments.

Reporting for specific materials, systems and methods

Materials & experimental systems

n/a	Involvement in the study
<input checked="" type="checkbox"/>	<input type="checkbox"/> Unique biological materials
<input checked="" type="checkbox"/>	<input type="checkbox"/> Antibodies
<input checked="" type="checkbox"/>	<input type="checkbox"/> Eukaryotic cell lines
<input checked="" type="checkbox"/>	<input type="checkbox"/> Palaeontology
<input checked="" type="checkbox"/>	<input type="checkbox"/> Animals and other organisms
<input checked="" type="checkbox"/>	<input type="checkbox"/> Human research participants

Methods

n/a	Involvement in the study
<input checked="" type="checkbox"/>	<input type="checkbox"/> ChIP-seq
<input checked="" type="checkbox"/>	<input type="checkbox"/> Flow cytometry
<input checked="" type="checkbox"/>	<input type="checkbox"/> MRI-based neuroimaging